Available online at www.sciencedirect.com
ScienceDirect
Comput. Methods Appl. Mech. Engrg. 296 (2015) 248–272
Computer methods in applied mechanics and engineering
www.elsevier.com/locate/cma

An extended range of stable-symmetric-conservative Flux Reconstruction correction functions

P.E. Vincent[a,*], A.M. Farrington[a], F.D. Witherden[a], A. Jameson[b]

[a] *Department of Aeronautics, Imperial College London, South Kensington, London, SW7 2AZ, UK*
[b] *Department of Aeronautics and Astronautics, Stanford University, Stanford, CA, 94305, USA*

Received 23 January 2015; received in revised form 11 June 2015; accepted 23 July 2015
Available online 4 August 2015

Abstract

The Flux Reconstruction (FR) approach offers an efficient route to achieving high-order accuracy on unstructured grids. Additionally, FR offers a flexible framework for defining a range of numerical schemes in terms of so-called FR correction functions. Recently, a one-parameter family of FR correction functions were identified that lead to stable schemes for 1D linear advection problems. In this study we develop a procedure for identifying an extended range of stable, symmetric, and conservative FR correction functions. The procedure is applied to identify ranges of such correction functions for various orders of accuracy. Numerical experiments are undertaken, and the results found to be in agreement with the theoretical findings.

Keywords: High-order methods; Flux Reconstruction; Discontinuous Galerkin method; Spectral difference method; Energy stability

1. Introduction

High-order methods for computational aerodynamics on unstructured grids offer the promise of increased accuracy at reduced cost, within the vicinity of complex engineering geometries. As such they have garnered continued interest over the past decades. However, to-date, their 'real-world' adoption in both industry and academia remains limited [1]. In 2007 Huynh proposed the Flux Reconstruction (FR) approach to high-order methods [2]. Based on a differential form of the governing system, it is hoped FR (also referred to as Lifting Collocation Penalty [3] or Correction Procedure via Reconstruction [4]) will facilitate adoption of high-order methods amongst a wider community of fluid dynamicists.

Various properties of FR schemes, including their dispersion and dissipation characteristics [5,6], their associated Courant–Friedrichs–Lewy (CFL) limit [2,5], and their fundamental stability [7], are all determined in full or in part by the form of their associated FR correction functions. These correction functions act to lift inter-element flux jumps from the boundary into the interior of each element. Building on the work of Huynh [2] and Jameson [8],

* Corresponding author. Tel.: +44 0 20 759 41975.
E-mail address: p.vincent@imperial.ac.uk (P.E. Vincent).

http://dx.doi.org/10.1016/j.cma.2015.07.023

Vincent, Castonguay and Jameson recently identified a one-parameter family of correction functions that lead to stable FR schemes for 1D linear advection problems [7]. Identification of these correction functions, henceforth referred to as Vincent–Castonguay–Jameson–Huynh (VCJH) correction functions, provided significant insight into stability properties various FR schemes. However, further work is required in order to determine a full specification of the necessary and sufficient conditions that should be imposed on correction functions in order to guarantee stability.

In this study we develop a procedure for identifying an extended range of stable, symmetric, and conservative FR correction functions. The procedure is applied to identify ranges of such correction functions for various orders or accuracy. In all cases the original one-parameter VCJH correction functions are found to be a sub-set of the extended ranges. Numerical experiments are undertaken in order to verify the theoretical findings.

2. Flux reconstruction

2.1. Overview

FR schemes are similar to nodal DG schemes, which are arguably the most popular type of unstructured high-order method (at least in the field of computational aerodynamics). Like nodal DG schemes, FR schemes utilise a high-order (nodal) polynomial basis to approximate the solution within each element of the computational domain, and like nodal DG schemes, FR schemes do not explicitly enforce inter-element solution continuity. However, unlike nodal DG schemes, FR methods are based solely on the governing system in a differential form. A description of the FR approach in 1D is presented below. For further information see the original paper of Huynh [2].

2.2. Preliminaries

Consider solving the following 1D scalar conservation law

$$\frac{\partial u}{\partial t} + \frac{\partial f}{\partial x} = 0 \tag{2.1}$$

within an arbitrary domain $\boldsymbol{\Omega}$, where x is a spatial coordinate, t is time, $u = u(x, t)$ is a conserved scalar quantity and $f = f(u)$ is the flux of u in the x direction. Additionally, consider partitioning $\boldsymbol{\Omega}$ into N distinct elements, each denoted $\boldsymbol{\Omega}_n = \{x | x_n < x < x_{n+1}\}$, such that

$$\boldsymbol{\Omega} = \bigcup_{n=0}^{N-1} \boldsymbol{\Omega}_n, \qquad \bigcap_{n=0}^{N-1} \boldsymbol{\Omega}_n = \emptyset. \tag{2.2}$$

The FR approach requires u is approximated in each $\boldsymbol{\Omega}_n$ by a function $u_n^\delta = u_n^\delta(x, t)$, which is a polynomial of degree k within $\boldsymbol{\Omega}_n$, and identically zero elsewhere. Additionally, the FR approach requires f is approximated in each $\boldsymbol{\Omega}_n$ by a function $f_n^\delta = f_n^\delta(x, t)$, which is a polynomial of degree $k + 1$ within $\boldsymbol{\Omega}_n$, and identically zero elsewhere. Consequently, when employing the FR approach, a total approximate solution $u^\delta = u^\delta(x, t)$ and a total approximate flux $f^\delta = f^\delta(x, t)$ can be defined within $\boldsymbol{\Omega}$ as

$$u^\delta = \sum_{n=0}^{N-1} u_n^\delta \approx u, \qquad f^\delta = \sum_{n=0}^{N-1} f_n^\delta \approx f, \tag{2.3}$$

where no level of inter-element continuity in u^δ is explicitly enforced. However, f^δ is required to be C_0 continuous at element interfaces.

Note the requirement that each f_n^δ is one degree higher than each u_n^δ, which consequently ensures the divergence of f_n^δ is of the same degree as u_n^δ within $\boldsymbol{\Omega}_n$.

2.3. Implementation

From an implementation perspective, it is advantageous to transform each $\boldsymbol{\Omega}_n$ to a standard element $\boldsymbol{\Omega}_S = \{\hat{x} | -1 \leq \hat{x} \leq 1\}$ via the mapping

$$\hat{x} = \Gamma_n(x) = 2\left(\frac{x - x_n}{x_{n+1} - x_n}\right) - 1, \tag{2.4}$$

which has the inverse

$$x = \Gamma_n^{-1}(\hat{x}) = \left(\frac{1-\hat{x}}{2}\right) x_n + \left(\frac{1+\hat{x}}{2}\right) x_{n+1}. \tag{2.5}$$

Having performed such a transformation, the evolution of u_n^δ within any individual $\boldsymbol{\Omega}_n$ (and thus the evolution of u^δ within $\boldsymbol{\Omega}$) can be determined by solving the following transformed equation within the standard element $\boldsymbol{\Omega}_S$

$$\frac{\partial \hat{u}^\delta}{\partial t} + \frac{\partial \hat{f}^\delta}{\partial \hat{x}} = 0, \tag{2.6}$$

where

$$\hat{u}^\delta = \hat{u}^\delta(\hat{x}, t) = u_n^\delta(\Gamma_n^{-1}(\hat{x}), t) \tag{2.7}$$

is a polynomial of degree k,

$$\hat{f}^\delta = \hat{f}^\delta(\hat{x}, t) = \frac{f_n^\delta(\Gamma_n^{-1}(\hat{x}), t)}{J_n}, \tag{2.8}$$

is a polynomial of degree $k+1$, and $J_n = (x_{n+1} - x_n)/2$.

The FR approach to solving Eq. (2.6) within the standard element $\boldsymbol{\Omega}_S$ can be described in five stages. The first stage involves representing $\hat{u}^\delta$ in terms of a nodal basis as follows:

$$\hat{u}^\delta = \sum_{i=0}^{k} \hat{u}_i^\delta \, l_i, \tag{2.9}$$

where l_i are Lagrange polynomials defined as

$$l_i = \prod_{j=0, j\neq i}^{k} \left(\frac{\hat{x} - \hat{x}_j}{\hat{x}_i - \hat{x}_j}\right), \tag{2.10}$$

$\hat{x}_i$ ($i = 0$ to k) are $k+1$ distinct solution points within $\boldsymbol{\Omega}_S$, and $\hat{u}_i^\delta = \hat{u}_i^\delta(t)$ ($i = 0$ to k) are values of $\hat{u}^\delta$ at the solution points $\hat{x}_i$.

The second stage of the FR approach involves constructing a degree k polynomial $\hat{f}^{\delta D} = \hat{f}^{\delta D}(\hat{x}, t)$, defined as the approximate transformed discontinuous flux within $\boldsymbol{\Omega}_S$. Specifically, $\hat{f}^{\delta D}$ is obtained via a collocation projection at the $k+1$ solution points, and can hence be expressed as

$$\hat{f}^{\delta D} = \sum_{i=0}^{k} \hat{f}_i^{\delta D} \, l_i \tag{2.11}$$

where the coefficients $\hat{f}_i^{\delta D} = \hat{f}_i^{\delta D}(t)$ are simply values of the transformed flux at each solution point $\hat{x}_i$ (evaluated directly from the approximate solution). The flux $\hat{f}^{\delta D}$ is termed discontinuous since it is calculated directly from the approximate solution, which is in general discontinuous between elements.

The third stage of the FR approach involves evaluating the approximate solution at either end of the standard element $\boldsymbol{\Omega}_S$ (*i.e.* at $\hat{x} = \pm 1$). These values, in conjunction with analogous information from adjoining elements, are then used to calculate numerical interface fluxes. The exact methodology for calculating such numerical interface fluxes will depend on the nature of the equations being solved. For example, when solving the Euler equations one may use a Roe type approximate Riemann solver [9], or any other two-point flux formula that provides for an upwind bias. In what follows the numerical interface fluxes associated with the left and right hand ends of $\boldsymbol{\Omega}_S$ (and transformed appropriately for use in $\boldsymbol{\Omega}_S$) will be denoted $\hat{f}_L^{\delta I}$ and $\hat{f}_R^{\delta I}$ respectively.

The penultimate stage of the FR approach involves constructing the degree $k+1$ polynomial $\hat{f}^\delta$, by adding a correction flux $\hat{f}^{\delta C} = \hat{f}^{\delta C}(\hat{x}, t)$ of degree $k+1$ to $\hat{f}^{\delta D}$, such that their sum equals the transformed numerical interface flux at $\hat{x} = \pm 1$, yet in some sense follows $\hat{f}^{\delta D}$ within the interior of $\boldsymbol{\Omega}_S$. In order to define $\hat{f}^{\delta C}$ such that it satisfies the above requirements, consider first defining degree $k+1$ correction functions $g_L = g_L(\hat{x})$ and $g_R = g_R(\hat{x})$

to approximate zero (in some sense) within $\boldsymbol{\Omega}_S$, as well as satisfying

$$g_L(-1) = 1, \qquad g_L(1) = 0, \tag{2.12}$$

$$g_R(-1) = 0, \qquad g_R(1) = 1, \tag{2.13}$$

and

$$g_L(\hat{x}) = g_R(-\hat{x}). \tag{2.14}$$

A suitable expression for $\hat{f}^{\delta C}$ can now be written in terms of g_L and g_R as

$$\hat{f}^{\delta C} = (\hat{f}_L^{\delta I} - \hat{f}_L^{\delta D})g_L + (\hat{f}_R^{\delta I} - \hat{f}_R^{\delta D})g_R, \tag{2.15}$$

where $\hat{f}_L^{\delta D} = \hat{f}^{\delta D}(-1, t)$ and $\hat{f}_R^{\delta D} = \hat{f}^{\delta D}(1, t)$. Using this expression, the degree $k + 1$ approximate transformed total flux $\hat{f}^{\delta}$ within $\boldsymbol{\Omega}_S$ can be constructed from the discontinuous and correction fluxes as follows:

$$\hat{f}^{\delta} = \hat{f}^{\delta D} + \hat{f}^{\delta C} = \hat{f}^{\delta D} + (\hat{f}_L^{\delta I} - \hat{f}_L^{\delta D})g_L + (\hat{f}_R^{\delta I} - \hat{f}_R^{\delta D})g_R. \tag{2.16}$$

The final stage of the FR approach involves evaluating the divergence of $\hat{f}^{\delta}$ at each solution point $\hat{x}_i$ using the expression

$$\frac{\partial \hat{f}^{\delta}}{\partial \hat{x}}(\hat{x}_i) = \sum_{j=0}^{k} \hat{f}_j^{\delta D} \frac{\mathrm{d}l_j}{\mathrm{d}\hat{x}}(\hat{x}_i) + (\hat{f}_L^{\delta I} - \hat{f}_L^{\delta D})\frac{\mathrm{d}g_L}{\mathrm{d}\hat{x}}(\hat{x}_i) + (\hat{f}_R^{\delta I} - \hat{f}_R^{\delta D})\frac{\mathrm{d}g_R}{\mathrm{d}\hat{x}}(\hat{x}_i). \tag{2.17}$$

These values can then be used to advance $\hat{u}^{\delta}$ in time via a suitable temporal discretisation of the following semi-discrete expression

$$\frac{\mathrm{d}\hat{u}_i^{\delta}}{\mathrm{d}t} = -\frac{\partial \hat{f}^{\delta}}{\partial \hat{x}}(\hat{x}_i). \tag{2.18}$$

2.4. Comments

The nature of a particular FR scheme depends on three factors, namely the location of the solution points $\hat{x}_i$, the methodology for calculating the interface fluxes $\hat{f}_L^{\delta I}$ and $\hat{f}_R^{\delta I}$, and the form of the correction functions g_L and g_R. Huynh [2] showed previously that a collocation based nodal DG scheme is recovered in 1D if the correction functions g_L and g_R are the right and left Radau polynomials respectively. Also, Huynh [2] showed that SD type methods can be recovered (at least for a linear flux function) if the correction functions g_L and g_R are set to zero at a set of k points within $\boldsymbol{\Omega}_S$ (located symmetrically about the origin).

Several additional forms of g_L and g_R were also suggested by Huynh [2], leading to the development of new schemes with various stability and accuracy properties. Building on this work, and the study of Jameson [8], Vincent, Castonguay and Jameson recently identified a one-parameter family of VCJH correction functions that lead to stable FR schemes for 1D linear advection problems [7].

3. Stable-symmetric-conservative correction functions

3.1. Preliminaries

If the $f(u) = au$ where a is a constant scalar (*i.e.* if the flux is linear), then Eq. (2.18) can be written as

$$\frac{\mathrm{d}\hat{u}_i^{\delta}}{\mathrm{d}t} = -\hat{a}\sum_{j=0}^{k} \hat{u}_j^{\delta} \frac{\mathrm{d}l_j}{\mathrm{d}\hat{x}}(\hat{x}_i) - (\hat{f}_L^{I} - \hat{a}\hat{u}_L^{\delta})\frac{\mathrm{d}g_L}{\mathrm{d}\hat{x}}(\hat{x}_i) - (\hat{f}_R^{I} - \hat{a}\hat{u}_R^{\delta})\frac{\mathrm{d}g_R}{\mathrm{d}\hat{x}}(\hat{x}_i), \tag{3.1}$$

where $\hat{a} = a/J_n$, $\hat{u}_L^{\delta} = \hat{u}^{\delta}(-1, t)$ and $\hat{u}_R^{\delta} = \hat{u}^{\delta}(1, t)$.

Eq. (3.1) can be written in matrix form as follows:

$$\frac{\mathrm{d}\hat{\mathbf{u}}^{\delta}}{\mathrm{d}t} = -\hat{a}\mathbf{D}\hat{\mathbf{u}}^{\delta} - (\hat{f}_L^{\delta I} - \hat{a}\hat{u}_L^{\delta})\mathbf{g}_{\hat{x}L} - (\hat{f}_R^{\delta I} - \hat{a}\hat{u}_R^{\delta})\mathbf{g}_{\hat{x}R}, \tag{3.2}$$

where

$$\hat{\mathbf{u}}^{\delta}[i] = \hat{u}_i^{\delta}, \tag{3.3}$$

$$\mathbf{g}_{\hat{x}L}[i] = \frac{\mathrm{d}g_L}{\mathrm{d}\hat{x}}(\hat{x}_i), \qquad \mathbf{g}_{\hat{x}R}[i] = \frac{\mathrm{d}g_R}{\mathrm{d}\hat{x}}(\hat{x}_i), \tag{3.4}$$

and

$$\mathbf{D}[i][j] = \frac{\mathrm{d}l_j}{\mathrm{d}\hat{x}}(\hat{x}_i). \tag{3.5}$$

On defining a Vandermonde matrix $\mathbf{V}$ as

$$\mathbf{V}[i][j] = L_j(\hat{x}_i), \tag{3.6}$$

where $L_j(\hat{x})$ is a Legendre polynomial of degree j (normalised to unity at $\hat{x} = 1$), one can multiplying through Eq. (3.2) from the left by $\mathbf{V}^{-1}$ to obtain

$$\frac{\mathrm{d}\mathbf{V}^{-1}\hat{\mathbf{u}}^{\delta}}{\mathrm{d}t} = -\hat{a}\mathbf{V}^{-1}\mathbf{D}\hat{\mathbf{u}}^{\delta} - (\hat{f}_L^{\delta I} - \hat{a}\hat{u}_L^{\delta})\mathbf{V}^{-1}\mathbf{g}_{\hat{x}L} - (\hat{f}_R^{\delta I} - \hat{a}\hat{u}_R^{\delta})\mathbf{V}^{-1}\mathbf{g}_{\hat{x}R}, \tag{3.7}$$

and thus

$$\frac{\mathrm{d}\mathbf{V}^{-1}\hat{\mathbf{u}}^{\delta}}{\mathrm{d}t} = -\hat{a}\mathbf{V}^{-1}\mathbf{D}\mathbf{V}\mathbf{V}^{-1}\hat{\mathbf{u}}^{\delta} - (\hat{f}_L^{\delta I} - \hat{a}\hat{u}_L^{\delta})\mathbf{V}^{-1}\mathbf{g}_{\hat{x}L} - (\hat{f}_R^{\delta I} - \hat{a}\hat{u}_R^{\delta})\mathbf{V}^{-1}\mathbf{g}_{\hat{x}R}, \tag{3.8}$$

which can be written as

$$\frac{\mathrm{d}\tilde{\hat{\mathbf{u}}}^{\delta}}{\mathrm{d}t} = -\hat{a}\tilde{\mathbf{D}}\tilde{\hat{\mathbf{u}}}^{\delta} - (\hat{f}_L^{\delta I} - \hat{a}\hat{u}_L^{\delta})\tilde{\mathbf{g}}_{\hat{x}L} - (\hat{f}_R^{\delta I} - \hat{a}\hat{u}_R^{\delta})\tilde{\mathbf{g}}_{\hat{x}R}, \tag{3.9}$$

where

$$\tilde{\hat{\mathbf{u}}}^{\delta} = \mathbf{V}^{-1}\hat{\mathbf{u}}^{\delta}, \qquad \tilde{\mathbf{g}}_{\hat{x}L} = \mathbf{V}^{-1}\mathbf{g}_{\hat{x}L}, \qquad \tilde{\mathbf{g}}_{\hat{x}R} = \mathbf{V}^{-1}\mathbf{g}_{\hat{x}R}, \tag{3.10}$$

are vectors of modal Legendre expansion coefficient for the solution, left correction function derivative, and right correction function derivative respectively, and

$$\tilde{\mathbf{D}} = \mathbf{V}^{-1}\mathbf{D}\mathbf{V} \tag{3.11}$$

is the modal Legendre differentiation matrix.

3.2. Stability

Theorem 1. *For all k, 1D FR correction functions are stable for a linear flux if*

$$\tilde{\mathbf{g}}_{\hat{x}L} = -(\tilde{\mathbf{M}} + \tilde{\mathbf{Q}})^{-1}\tilde{\mathbf{L}}, \tag{3.12}$$

$$\tilde{\mathbf{g}}_{\hat{x}R} = (\tilde{\mathbf{M}} + \tilde{\mathbf{Q}})^{-1}\tilde{\mathbf{R}}, \tag{3.13}$$

where $\tilde{\mathbf{M}}$ *is the modal Legendre mass matrix defined as*

$$\tilde{\mathbf{M}}[i][j] = \int_{-1}^{1} L_i L_j \mathrm{d}\hat{x}, \tag{3.14}$$

$\tilde{\mathbf{Q}}$ *is a real square matrix of dimension* $k+1$ *that satisfies*

$$\tilde{\mathbf{Q}} = \tilde{\mathbf{Q}}^T, \tag{3.15}$$

$$\tilde{\mathbf{Q}}\tilde{\mathbf{D}} + \tilde{\mathbf{D}}^T\tilde{\mathbf{Q}}^T = 0, \tag{3.16}$$

$$\tilde{\mathbf{M}} + \tilde{\mathbf{Q}} > 0, \tag{3.17}$$

and $\tilde{\mathbf{L}}$ *and* $\tilde{\mathbf{R}}$ *are defined as*

$$\tilde{\mathbf{L}}[i] = L_i(-1) = (-1)^i, \qquad \tilde{\mathbf{R}}[i] = L_i(1) = 1. \tag{3.18}$$

Proof. On multiplying Eq. (3.9) from the left by $\tilde{\hat{\mathbf{u}}}^{\delta T}(\tilde{\mathbf{M}} + \tilde{\mathbf{Q}})$ one obtains

$$\begin{aligned}\tilde{\hat{\mathbf{u}}}^{\delta T}(\tilde{\mathbf{M}} + \tilde{\mathbf{Q}})\frac{\mathrm{d}\tilde{\hat{\mathbf{u}}}^{\delta}}{\mathrm{d}t} &= -\hat{a}\tilde{\hat{\mathbf{u}}}^{\delta T}\tilde{\mathbf{M}}\tilde{\mathbf{D}}\tilde{\hat{\mathbf{u}}}^{\delta} - \hat{a}\tilde{\hat{\mathbf{u}}}^{\delta T}\tilde{\mathbf{Q}}\tilde{\mathbf{D}}\tilde{\hat{\mathbf{u}}}^{\delta} \\ &\quad - (\hat{f}_L^{\delta I} - \hat{a}\hat{u}_L^{\delta})\tilde{\hat{\mathbf{u}}}^{\delta T}(\tilde{\mathbf{M}} + \tilde{\mathbf{Q}})\tilde{\mathbf{g}}_{\hat{x}L} - (\hat{f}_R^{\delta I} - \hat{a}\hat{u}_R^{\delta})\tilde{\hat{\mathbf{u}}}^{\delta T}(\tilde{\mathbf{M}} + \tilde{\mathbf{Q}})\tilde{\mathbf{g}}_{\hat{x}R}.\end{aligned} \tag{3.19}$$

Eq. (3.15) implies that $\tilde{\mathbf{M}} + \tilde{\mathbf{Q}}$ is symmetric, hence (3.19) can be written as

$$\begin{aligned}\frac{1}{2}\frac{\mathrm{d}}{\mathrm{d}t}\tilde{\hat{\mathbf{u}}}^{\delta T}(\tilde{\mathbf{M}} + \tilde{\mathbf{Q}})\tilde{\hat{\mathbf{u}}}^{\delta} &= -\hat{a}\tilde{\hat{\mathbf{u}}}^{\delta T}\tilde{\mathbf{M}}\tilde{\mathbf{D}}\tilde{\hat{\mathbf{u}}}^{\delta} - \hat{a}\tilde{\hat{\mathbf{u}}}^{\delta T}\tilde{\mathbf{Q}}\tilde{\mathbf{D}}\tilde{\hat{\mathbf{u}}}^{\delta} \\ &\quad - (\hat{f}_L^{\delta I} - \hat{a}\hat{u}_L^{\delta})\tilde{\hat{\mathbf{u}}}^{\delta T}(\tilde{\mathbf{M}} + \tilde{\mathbf{Q}})\tilde{\mathbf{g}}_{\hat{x}L} - (\hat{f}_R^{\delta I} - \hat{a}\hat{u}_R^{\delta})\tilde{\hat{\mathbf{u}}}^{\delta T}(\tilde{\mathbf{M}} + \tilde{\mathbf{Q}})\tilde{\mathbf{g}}_{\hat{x}R}.\end{aligned} \tag{3.20}$$

Eq. (3.16) implies that $\tilde{\mathbf{Q}}\tilde{\mathbf{D}}$ is anti-symmetric and hence

$$\tilde{\hat{\mathbf{u}}}^{\delta T}\tilde{\mathbf{Q}}\tilde{\mathbf{D}}\tilde{\hat{\mathbf{u}}}^{\delta} = 0, \tag{3.21}$$

and Eq. (3.17) implies that

$$\tilde{\hat{\mathbf{u}}}^{\delta T}(\tilde{\mathbf{M}} + \tilde{\mathbf{Q}})\tilde{\mathbf{g}}_{\hat{x}L} = -\hat{u}_L^{\delta}, \qquad \tilde{\hat{\mathbf{u}}}^{\delta T}(\tilde{\mathbf{M}} + \tilde{\mathbf{Q}})\tilde{\mathbf{g}}_{\hat{x}R} = \hat{u}_R^{\delta}. \tag{3.22}$$

Hence, Eq. (3.20) can be written as

$$\frac{1}{2}\frac{\mathrm{d}}{\mathrm{d}t}\tilde{\hat{\mathbf{u}}}^{\delta T}(\tilde{\mathbf{M}} + \tilde{\mathbf{Q}})\tilde{\hat{\mathbf{u}}}^{\delta} = -\hat{a}\tilde{\hat{\mathbf{u}}}^{\delta T}\tilde{\mathbf{M}}\tilde{\mathbf{D}}\tilde{\hat{\mathbf{u}}}^{\delta} + (\hat{f}_L^{\delta I} - \hat{a}\hat{u}_L^{\delta})\hat{u}_L^{\delta} - (\hat{f}_R^{\delta I} - \hat{a}\hat{u}_R^{\delta})\hat{u}_R^{\delta}, \tag{3.23}$$

which using the fact that

$$\tilde{\hat{\mathbf{u}}}^{\delta T}\tilde{\mathbf{M}}\tilde{\mathbf{D}}\tilde{\hat{\mathbf{u}}}^{\delta} = \int_{-1}^{1}\hat{u}^{\delta}\frac{\mathrm{d}\hat{u}^{\delta}}{\mathrm{d}\hat{x}}\,\mathrm{d}\hat{x} = \frac{1}{2}(\hat{u}_R^{\delta 2} - \hat{u}_L^{\delta 2}), \tag{3.24}$$

can be written as

$$\frac{\mathrm{d}}{\mathrm{d}t}\tilde{\hat{\mathbf{u}}}^{\delta T}(\tilde{\mathbf{M}} + \tilde{\mathbf{Q}})\tilde{\hat{\mathbf{u}}}^{\delta} = (2\hat{f}_L^{\delta I} - \hat{a}\hat{u}_L^{\delta})\hat{u}_L^{\delta} - (2\hat{f}_R^{\delta I} - \hat{a}\hat{u}_R^{\delta})\hat{u}_R^{\delta}, \tag{3.25}$$

and hence

$$\frac{\mathrm{d}}{\mathrm{d}t}\hat{\mathbf{u}}^{\delta T}\mathbf{V}^{-T}(\tilde{\mathbf{M}} + \tilde{\mathbf{Q}})\mathbf{V}^{-1}\hat{\mathbf{u}}^{\delta} = (2\hat{f}_L^{\delta I} - \hat{a}\hat{u}_L^{\delta})\hat{u}_L^{\delta} - (2\hat{f}_R^{\delta I} - \hat{a}\hat{u}_R^{\delta})\hat{u}_R^{\delta}. \tag{3.26}$$

On rewriting Eq. (3.26) in terms of physical space quantities from the nth element one obtains

$$\begin{aligned}&\frac{\mathrm{d}}{\mathrm{d}t}\mathbf{u}_n^{\delta T}\mathbf{V}^{-T}(\tilde{\mathbf{M}} + \tilde{\mathbf{Q}})\mathbf{V}^{-1}\mathbf{u}_n^{\delta} \\ &\quad = \frac{1}{J_n}[2f_n^{\delta I} - au_n^{\delta}(x_n)]u_n^{\delta}(x_n) - \frac{1}{J_n}[2f_{n+1}^{\delta I} - au_n^{\delta}(x_{n+1})]u_n^{\delta}(x_{n+1}),\end{aligned} \tag{3.27}$$

and hence

$$\begin{aligned}&\frac{\mathrm{d}}{\mathrm{d}t}J_n\mathbf{u}_n^{\delta T}\mathbf{V}^{-T}(\tilde{\mathbf{M}} + \tilde{\mathbf{Q}})\mathbf{V}^{-1}\mathbf{u}_n^{\delta} \\ &\quad = [2f_n^{\delta I} - au_n^{\delta}(x_n)]u_n^{\delta}(x_n) - [2f_{n+1}^{\delta I} - au_n^{\delta}(x_{n+1})]u_n^{\delta}(x_{n+1}),\end{aligned} \tag{3.28}$$

where $\mathbf{u}_n^\delta$ is a vector of the physical solution at the solution points inside the nth element, and $f_n^{\delta I}$ and $f_{n+1}^{\delta I}$ are physical numerical interface fluxes evaluated at x_n and x_{n+1} respectively. If the numerical flux at each internal interface x_n $(1 \leq n \leq N-1)$ is defined to have the form

$$f_n^{\delta I} = a\left[\frac{u_n^\delta(x_n) + u_{n-1}^\delta(x_n)}{2}\right] - |a|(1-\kappa)\left[\frac{u_n^\delta(x_n) - u_{n-1}^\delta(x_n)}{2}\right], \tag{3.29}$$

where $0 \leq \kappa \leq 1$ (with $\kappa = 0$ recovering a fully upwind scheme, and $\kappa = 1$ recovering a central scheme), and if for simplicity the domain $\boldsymbol{\Omega}$ is assumed to be periodic such that

$$f_0^{\delta I} = f_N^{\delta I} = a\left[\frac{u_0^\delta(x_0) + u_{N-1}^\delta(x_N)}{2}\right] - |a|(1-\kappa)\left[\frac{u_0^\delta(x_0) - u_{N-1}^\delta(x_N)}{2}\right], \tag{3.30}$$

then summing Eq. (3.28) over all elements leads to

$$\begin{aligned}\frac{\mathrm{d}}{\mathrm{d}t}\|u^\delta\|^2 = &-\sum_{n=0}^{N-2}|a|(1-\kappa)[u_{n+1}^\delta(x_{n+1}) - u_n^\delta(x_{n+1})]^2 \\ &- |a|(1-\kappa)[u_0^\delta(x_0) - u_{N-1}^\delta(x_N)]^2,\end{aligned} \tag{3.31}$$

where

$$\|u^\delta\| = \sqrt{\sum_{n=0}^{N-1} J_n \mathbf{u}_n^{\delta T}\mathbf{V}^{-T}(\tilde{\mathbf{M}} + \tilde{\mathbf{Q}})\mathbf{V}^{-1}\mathbf{u}_n^\delta}, \tag{3.32}$$

which by Eq. (3.17) is a broken norm of the solution. Finally, since $0 \leq \kappa \leq 1$, Eq. (3.31) implies

$$\frac{\mathrm{d}}{\mathrm{d}t}\|u^\delta\|^2 \leq 0, \tag{3.33}$$

hence the broken norm $\|u^\delta\|$ will remain bounded, and hence all norms of the solution will remain bounded via equivalence of norms in a finite dimensional space. □

3.3. Symmetry

Theorem 2. *For all k, 1D FR correction functions of the form defined by Eqs. (3.12) and (3.13) are symmetric if*

$$\tilde{\mathbf{J}}\tilde{\mathbf{Q}} = \tilde{\mathbf{Q}}\tilde{\mathbf{J}}, \tag{3.34}$$

where

$$\tilde{\mathbf{J}}[i][j] = \delta_{ij}(-1)^{i+1} \quad 0 \leq i \leq k \quad 0 \leq j \leq k. \tag{3.35}$$

Proof. Given that $\tilde{\mathbf{M}}$ is diagonal, Eq. (3.34) implies

$$\tilde{\mathbf{J}}(\tilde{\mathbf{M}} + \tilde{\mathbf{Q}}) = (\tilde{\mathbf{M}} + \tilde{\mathbf{Q}})\tilde{\mathbf{J}}. \tag{3.36}$$

Using $\tilde{\mathbf{J}}^{-1} = \tilde{\mathbf{J}}$ one obtains

$$(\tilde{\mathbf{M}} + \tilde{\mathbf{Q}})^{-1} = \tilde{\mathbf{J}}(\tilde{\mathbf{M}} + \tilde{\mathbf{Q}})^{-1}\tilde{\mathbf{J}}, \tag{3.37}$$

on multiplying from the right by $\tilde{\mathbf{L}}$ one obtains

$$(\tilde{\mathbf{M}} + \tilde{\mathbf{Q}})^{-1}\tilde{\mathbf{L}} = \tilde{\mathbf{J}}(\tilde{\mathbf{M}} + \tilde{\mathbf{Q}})^{-1}\tilde{\mathbf{J}}\tilde{\mathbf{L}}, \tag{3.38}$$

using $\tilde{\mathbf{R}} = -\tilde{\mathbf{J}}\tilde{\mathbf{L}}$ one obtains

$$-(\tilde{\mathbf{M}} + \tilde{\mathbf{Q}})^{-1}\tilde{\mathbf{L}} = \tilde{\mathbf{J}}(\tilde{\mathbf{M}} + \tilde{\mathbf{Q}})^{-1}\tilde{\mathbf{R}}, \tag{3.39}$$

finally using Eqs. (3.12) and (3.13) one obtains

$$\tilde{\mathbf{g}}_{\hat{x}L} = \tilde{\mathbf{J}}\tilde{\mathbf{g}}_{\hat{x}R}, \tag{3.40}$$

and hence

$$\tilde{\mathbf{g}}_{\hat{x}L}[i] = (-1)^{i+1}\tilde{\mathbf{g}}_{\hat{x}R}[i] \quad 0 \leq i \leq k, \tag{3.41}$$

which implies symmetry since, as defined, $\tilde{\mathbf{g}}_{\hat{x}L}[i]$ and $\tilde{\mathbf{g}}_{\hat{x}R}[i]$ are the ith mode coefficients in a Legendre expansion of the left and right correction function derivatives respectively. □

3.4. Conservation

Theorem 3. *For all k, 1D FR correction functions of the form defined by Eqs. (3.12) and (3.13) are conservative if*

$$\tilde{\mathbf{g}}_{\hat{x}L}[0] = -\frac{1}{2}, \qquad \tilde{\mathbf{g}}_{\hat{x}R}[0] = \frac{1}{2}, \tag{3.42}$$

where, as defined, $\tilde{\mathbf{g}}_{\hat{x}L}[0]$ and $\tilde{\mathbf{g}}_{\hat{x}R}[0]$ are the zero mode coefficients in a Legendre expansion of the left and right correction function derivatives respectively.

Proof. Using the orthogonality of Legendre polynomials, Eq. (3.42) implies

$$\begin{aligned} g_L(1) - g_L(-1) &= \int_{-1}^{1} \frac{\mathrm{d}g_L}{\mathrm{d}\hat{x}}\,\mathrm{d}\hat{x} = \tilde{\mathbf{g}}_{\hat{x}L}[0]\int_{-1}^{1} L_0\,\mathrm{d}\hat{x} = -1, \\ g_R(1) - g_R(-1) &= \int_{-1}^{1} \frac{\mathrm{d}g_R}{\mathrm{d}\hat{x}}\,\mathrm{d}\hat{x} = \tilde{\mathbf{g}}_{\hat{x}R}[0]\int_{-1}^{1} L_0\,\mathrm{d}\hat{x} = 1. \end{aligned} \tag{3.43}$$

If $g_L(-1) = 1$ then Eq. (3.43) implies that $g_L(1) = 0$, and if $g_R(1) = 1$ then Eq. (3.43) implies that $g_R(-1) = 0$. Hence the schemes will be conservative. □

3.5. Summary

For all k, correction functions defined by Eqs. (3.12) and (3.13) will be stable, symmetric and conservative provided the conditions defined by Eqs. (3.15)–(3.17), (3.34) and (3.42) are satisfied.

4. Identifying stable-symmetric-conservative correction functions when $k = 3$

4.1. Derivation

For reference, when $k = 3$

$$\tilde{\mathbf{M}} = \begin{bmatrix} 2 & 0 & 0 & 0 \\ 0 & \frac{2}{3} & 0 & 0 \\ 0 & 0 & \frac{2}{5} & 0 \\ 0 & 0 & 0 & \frac{2}{7} \end{bmatrix}, \qquad \tilde{\mathbf{D}} = \begin{bmatrix} 0 & 1 & 0 & 1 \\ 0 & 0 & 3 & 0 \\ 0 & 0 & 0 & 5 \\ 0 & 0 & 0 & 0 \end{bmatrix}. \tag{4.1}$$

By inspection, the most general form of $\tilde{\mathbf{Q}}$ that simultaneously satisfies the stability conditions defined by Eqs. (3.15) and (3.16), and the symmetry condition defined by Eq. (3.34), is

$$\tilde{\mathbf{Q}} = \begin{bmatrix} 0 & 0 & 0 & 0 \\ 0 & 0 & 0 & -\frac{5}{3}q_1 \\ 0 & 0 & q_1 & 0 \\ 0 & -\frac{5}{3}q_1 & 0 & q_0 \end{bmatrix}. \tag{4.2}$$

Substituting Eq. (4.2) into Eqs. (3.12) and (3.13) leads to

$$\begin{aligned}
\mathbf{g}_{\hat{x}L}[0] &= -\frac{1}{2}, \\
\mathbf{g}_{\hat{x}L}[1] &= -\frac{3\,(21\,q_0 + 35\,q_1 + 6)}{\Xi}, \\
\mathbf{g}_{\hat{x}L}[2] &= -\frac{5}{5\,q_1 + 2}, \\
\mathbf{g}_{\hat{x}L}[3] &= -\frac{21\,(5\,q_1 + 2)}{\Xi},
\end{aligned} \tag{4.3}$$

and

$$\mathbf{g}_{\hat{x}R}[i] = (-1)^{i+1}\mathbf{g}_{\hat{x}L}[i] \quad 0 \leq i \leq 3, \tag{4.4}$$

where

$$\Xi = 175\,q_1^2 - 42\,q_0 - 12. \tag{4.5}$$

Eqs. (4.3) and (4.4) naturally satisfy the conservation conditions defined by Eq. (3.42). Finally, in order to satisfy the stability condition defined by Eq. (3.17), the matrix $\tilde{\mathbf{M}} + \tilde{\mathbf{Q}}$, and all three of its upper-left square sub-matrices, must have positive determinants, leading to the following constraints on q_0 and q_1

$$\begin{aligned}
&\frac{4}{3}\,q_1 + \frac{8}{15} > 0, \\
&-\frac{50}{9}\,q_1^3 + \frac{4}{21}\,(7\,q_0 + 2)\,q_1 - \frac{20}{9}\,q_1^2 + \frac{8}{15}\,q_0 + \frac{16}{105} > 0.
\end{aligned} \tag{4.6}$$

In summary, when $k = 3$, correction functions defined in terms of q_0 and q_1 via Eqs. (4.3) and (4.4) will result in stable FR schemes if q_0 and q_1 satisfy the constraints defined by Eq. (4.6). Examples of such correction functions are shown in Appendix A, Fig. 5. Also, for reference, the differential form of the norm defined by Eq. (3.32) when $k = 3$ is given in Appendix B, B.1.

4.2. Recovery of Vincent–Castonguay–Jameson–Huynh schemes

If $q_1 = 0$, then Eq. (4.3) collapses to

$$\mathbf{g}_{\hat{x}L}[0] = -\frac{1}{2}, \qquad \mathbf{g}_{\hat{x}L}[1] = \frac{3}{2}, \qquad \mathbf{g}_{\hat{x}L}[2] = -\frac{5}{2}, \qquad \mathbf{g}_{\hat{x}L}[3] = \frac{7}{7\,q_0 + 2}, \tag{4.7}$$

and Eq. (4.6) collapses to

$$q_0 > -\frac{2}{7}. \tag{4.8}$$

These define VCJH correction functions for $k = 3$, parameterised by q_0, with $q_0 = 0$ recovering a DG scheme, $q_0 = 3/14$ recovering the energy-stable SD scheme described by Jameson [8], and $q_0 = 8/21$ recovering the g_2 described by Huynh [2]. We note that this description of a VCJH correction function, in terms of a modal Legendre expansion of its derivative, is similar to that presented previously by Huynh [10].

4.3. Numerical experiments

Numerical experiments were undertaken to demonstrate that, when $k = 3$, correction functions defined in terms of q_0 and q_1 via Eqs. (4.3) and (4.4) result in stable FR schemes if q_0 and q_1 satisfy the constraints defined by Eq. (4.6).

Specifically, an equispaced sampling of 451 different schemes within a region of $q_0 - q_1$ space bounded by $-1 \leq q_0 \leq 4$ and $-1 \leq q_1 \leq 1$ were used to solve Eq. (2.1) with the following linear flux function

$$f(u) = u. \tag{4.9}$$

For each of the 451 numerical experiments the computational domain, defined as $\boldsymbol{\Omega} = [-1, 1]$, was subdivided into ten elements of equal size. A fully upwind flux was prescribed between adjoining elements. Gauss–Legendre points

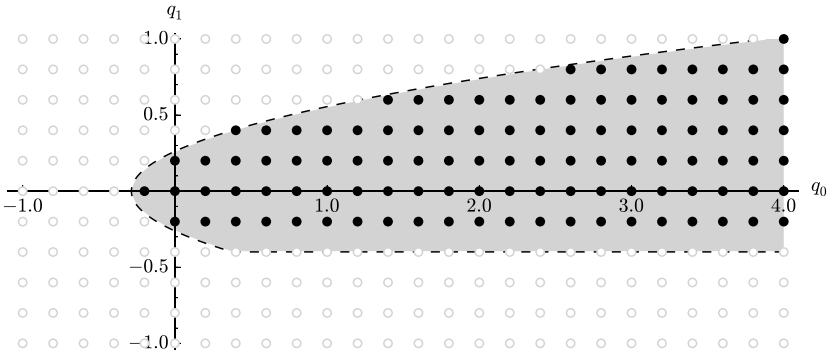

Fig. 1. Plot comparing theoretical and numerical results when $k = 3$. The shaded grey area bounded by a black dashed line highlights the theoretically stable region in $q_0 - q_1$ space. Solid circles denote schemes that were found to be numerically stable. Hollow circles denote schemes that were found to be numerically unstable.

were used as solution points within each element. Periodic boundary conditions were applied at the ends of $\boldsymbol{\Omega}$, and the following Gaussian profile was prescribed within $\boldsymbol{\Omega}$ at $t = 0$

$$u(x, 0) = e^{-20x^2}. \tag{4.10}$$

Time integration was performed using an explicit low-storage five-stage fourth-order Runge–Kutta method [11].

A scheme was deemed to be numerically unstable if the solution at any solution point attained a value of 1000 or greater before $t = 300$. Otherwise the scheme was deemed to be numerically stable. A plot illustrating which of the schemes were found to be numerically unstable, and which were found to be numerically stable, is shown in Fig. 1. Results of the numerical experiments are in agreement with the theoretical results of Section 4.1, since all schemes within the theoretically stable region of $q_0 - q_1$ space, defined by Eq. (4.6), were found to be numerically stable. Additionally, it can be seen that all schemes outside of the theoretically stable region were found to be numerically unstable.

5. Identifying stable-symmetric-conservative correction functions when $k = 4$

5.1. Derivation

For reference, when $k = 4$

$$\tilde{\mathbf{M}} = \begin{bmatrix} 2 & 0 & 0 & 0 & 0 \\ 0 & \frac{2}{3} & 0 & 0 & 0 \\ 0 & 0 & \frac{2}{5} & 0 & 0 \\ 0 & 0 & 0 & \frac{2}{7} & 0 \\ 0 & 0 & 0 & 0 & \frac{2}{9} \end{bmatrix}, \qquad \tilde{\mathbf{D}} = \begin{bmatrix} 0 & 1 & 0 & 1 & 0 \\ 0 & 0 & 3 & 0 & 3 \\ 0 & 0 & 0 & 5 & 0 \\ 0 & 0 & 0 & 0 & 7 \\ 0 & 0 & 0 & 0 & 0 \end{bmatrix}. \tag{5.1}$$

By inspection, the most general form of $\tilde{\mathbf{Q}}$ that simultaneously satisfies the stability conditions defined by Eqs. (3.15) and (3.16), and the symmetry condition defined by Eq. (3.34), is

$$\tilde{\mathbf{Q}} = \begin{bmatrix} 0 & 0 & 0 & 0 & \frac{35}{3} q_2 \\ 0 & 0 & 0 & -\frac{5}{3} q_2 & 0 \\ 0 & 0 & q_2 & 0 & -\frac{7}{5} q_1 - \frac{4}{3} q_2 \\ 0 & -\frac{5}{3} q_2 & 0 & q_1 & 0 \\ \frac{35}{3} q_2 & 0 & -\frac{7}{5} q_1 - \frac{4}{3} q_2 & 0 & q_0 \end{bmatrix}. \tag{5.2}$$

Substituting Eq. (5.2) into Eqs. (3.12) and (3.13) leads to

$$\begin{aligned}\mathbf{g}_{\hat{x}L}[0] &= \frac{175\,q_2\,f(q_1,q_2)}{g(q_0,q_1,q_2)} - \frac{1}{2},\\ \mathbf{g}_{\hat{x}R}[0] &= -\frac{175\,q_2\,f(q_1,q_2)}{g(q_0,q_1,q_2)} + \frac{1}{2},\end{aligned} \tag{5.3}$$

and

$$\mathbf{g}_{\hat{x}L}[1] = \mathbf{g}_{\hat{x}R}[1] = \frac{h(q_1,q_2)}{f(q_1,q_2)}, \tag{5.4}$$

where the specific forms of $f(q_1,q_2)$, $g(q_0,q_1,q_2)$ and $h(q_1,q_2)$ are omitted for brevity. In order for Eq. (5.3) to satisfy the conservation conditions defined by Eq. (3.42) it is required that $q_2 f(q_1,q_2) = 0$, which requires $q_2 = 0$ so that the denominator in (5.4) is non-zero. Substituting Eq. (5.2) into Eqs. (3.12) and (3.13) with $q_2 = 0$ leads to

$$\begin{aligned}\mathbf{g}_{\hat{x}L}[0] &= -\frac{1}{2},\\ \mathbf{g}_{\hat{x}L}[1] &= \frac{3}{2},\\ \mathbf{g}_{\hat{x}L}[2] &= \frac{5\,(45\,q_0 + 63\,q_1 + 10)}{\Xi},\\ \mathbf{g}_{\hat{x}L}[3] &= \frac{7}{7\,q_1 + 2},\\ \mathbf{g}_{\hat{x}L}[4] &= \frac{45\,(7\,q_1 + 2)}{\Xi},\end{aligned} \tag{5.5}$$

and

$$\mathbf{g}_{\hat{x}R}[i] = (-1)^{i+1}\mathbf{g}_{\hat{x}L}[i] \quad 0 \le i \le 4, \tag{5.6}$$

where

$$\Xi = 441\,q_1^2 - 90\,q_0 - 20. \tag{5.7}$$

Finally, in order to satisfy the stability condition defined by Eq. (3.17), the matrix $\tilde{\mathbf{M}} + \tilde{\mathbf{Q}}$, and all four of its upper-left square sub-matrices, must have positive determinants, leading to the following constraints on q_0 and q_1

$$\begin{aligned}&\frac{8}{15}\,q_1 + \frac{16}{105} > 0,\\ &-\frac{196}{75}\,q_1^3 + \frac{8}{135}\,(9\,q_0 + 2)\,q_1 - \frac{56}{75}\,q_1^2 + \frac{16}{105}\,q_0 + \frac{32}{945} > 0.\end{aligned} \tag{5.8}$$

In summary, when $k = 4$, correction functions defined in terms of q_0 and q_1 via Eqs. (5.5) and (5.6) will result in stable FR schemes if q_0 and q_1 satisfy the constraints defined by Eq. (5.8). Examples of such correction functions are shown in Appendix A, Fig. 6. Also, for reference, the differential form of the norm defined by Eq. (3.32) when $k = 4$ is given in Appendix B, B.2.

5.2. Recovery of Vincent–Castonguay–Jameson–Huynh schemes

If $q_1 = 0$, then Eq. (5.5) collapses to

$$\begin{aligned}&\mathbf{g}_{\hat{x}L}[0] = -\frac{1}{2}, \quad \mathbf{g}_{\hat{x}L}[1] = \frac{3}{2}, \quad \mathbf{g}_{\hat{x}L}[2] = -\frac{5}{2}, \quad \mathbf{g}_{\hat{x}L}[3] = \frac{7}{2},\\ &\mathbf{g}_{\hat{x}L}[4] = -\frac{9}{9\,q_0 + 2},\end{aligned} \tag{5.9}$$

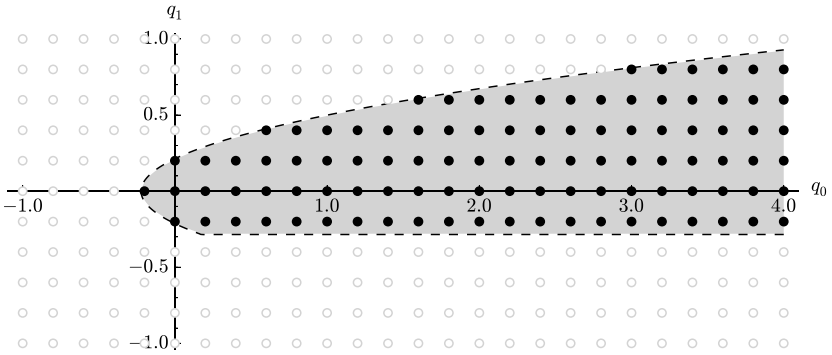

Fig. 2. Plot comparing theoretical and numerical results when $k = 4$. The shaded grey area bounded by a black dashed line highlights the theoretically stable region in $q_0 - q_1$ space. Solid circles denote schemes that were found to be numerically stable. Hollow circles denote schemes that were found to be numerically unstable.

and Eq. (5.8) collapses to

$$q_0 > -\frac{2}{9}. \tag{5.10}$$

These define VCJH correction functions for $k = 4$, parameterised by q_0, with $q_0 = 0$ recovering a DG scheme, $q_0 = 8/45$ recovering the energy-stable SD scheme described by Jameson [8], and $q_0 = 5/18$ recovering the g_2 described by Huynh [2]. We note that this description of a VCJH correction function, in terms of a modal Legendre expansion of its derivative, is similar to that presented previously by Huynh [10].

5.3. Numerical experiments

Numerical experiments were undertaken to demonstrate that, when $k = 4$, correction functions defined in terms of q_0 and q_1 via Eqs. (5.5) and (5.6) result in stable FR schemes if q_0 and q_1 satisfy the constraints defined by Eq. (5.8).

Specifically, an equispaced sampling of 451 different schemes within a region of $q_0 - q_1$ space bounded by $-1 \leq q_0 \leq 4$ and $-1 \leq q_1 \leq 1$ were used to solve Eq. (2.1) with the flux function defined by Eq. (4.9). For each of the 451 numerical experiments the setup was identical to that described in Section 4.3. A scheme was deemed to be numerically unstable if the solution at any solution point attained a value of 1000 or greater before $t = 300$. Otherwise the scheme was deemed to be numerically stable. A plot illustrating which of the schemes were found to be numerically unstable, and which were found to be numerically stable, is shown in Fig. 2. Results of the numerical experiments are in agreement with the theoretical results of Section 5.1, since all schemes within the theoretically stable region of $q_0 - q_1$ space, defined by Eq. (5.8), were found to be numerically stable. Additionally, it can be seen that all schemes outside of the theoretically stable region were found to be numerically unstable.

6. Identifying stable-symmetric-conservative correction functions when $k = 5$

6.1. Derivation

For reference, when $k = 5$

$$\tilde{\mathbf{M}} = \begin{bmatrix} 2 & 0 & 0 & 0 & 0 & 0 \\ 0 & \frac{2}{3} & 0 & 0 & 0 & 0 \\ 0 & 0 & \frac{2}{5} & 0 & 0 & 0 \\ 0 & 0 & 0 & \frac{2}{7} & 0 & 0 \\ 0 & 0 & 0 & 0 & \frac{2}{9} & 0 \\ 0 & 0 & 0 & 0 & 0 & \frac{2}{11} \end{bmatrix}, \qquad \tilde{\mathbf{D}} = \begin{bmatrix} 0 & 1 & 0 & 1 & 0 & 1 \\ 0 & 0 & 3 & 0 & 3 & 0 \\ 0 & 0 & 0 & 5 & 0 & 5 \\ 0 & 0 & 0 & 0 & 7 & 0 \\ 0 & 0 & 0 & 0 & 0 & 9 \\ 0 & 0 & 0 & 0 & 0 & 0 \end{bmatrix}. \tag{6.1}$$

By inspection, the most general form of $\tilde{\mathbf{Q}}$ that simultaneously satisfies the stability conditions defined by Eqs. (3.15) and (3.16), and the symmetry condition defined by Eq. (3.34), is

$$\tilde{\mathbf{Q}} = \begin{bmatrix} 0 & 0 & 0 & 0 & 0 & 0 \\ 0 & 0 & 0 & 0 & 0 & \frac{21}{5} q_2 \\ 0 & 0 & 0 & 0 & -\frac{7}{5} q_2 & 0 \\ 0 & 0 & 0 & q_2 & 0 & -\frac{9}{7} q_1 - \frac{4}{5} q_2 \\ 0 & 0 & -\frac{7}{5} q_2 & 0 & q_1 & 0 \\ 0 & \frac{21}{5} q_2 & 0 & -\frac{9}{7} q_1 - \frac{4}{5} q_2 & 0 & q_0 \end{bmatrix}. \tag{6.2}$$

Substituting Eq. (6.2) into Eqs. (3.12) and (3.13) leads to

$$\begin{aligned} \mathbf{g}_{\hat{x}L}[0] &= -\frac{1}{2}, \\ \mathbf{g}_{\hat{x}L}[1] &= \frac{15\left(4455 q_1^2 - 7\left(385 q_0 - 2871 q_1 - 392\right) q_2 + 22099 q_2^2 - 770 q_0 - 140\right)}{\Xi}, \\ \mathbf{g}_{\hat{x}L}[2] &= \frac{5\left(45 q_1 + 63 q_2 + 10\right)}{441 q_2^2 - 90 q_1 - 20}, \\ \mathbf{g}_{\hat{x}L}[3] &= \frac{35\left(77\left(81 q_1 - 8\right) q_2 + 24255 q_2^2 - 770 q_0 - 990 q_1 - 140\right)}{\Xi}, \\ \mathbf{g}_{\hat{x}L}[4] &= \frac{45\left(7 q_2 + 2\right)}{441 q_2^2 - 90 q_1 - 20}, \\ \mathbf{g}_{\hat{x}L}[5] &= \frac{385\left(441 q_2^2 - 90 q_1 - 20\right)}{\Xi}, \end{aligned} \tag{6.3}$$

and

$$\mathbf{g}_{\hat{x}R}[i] = (-1)^{i+1} \mathbf{g}_{\hat{x}L}[i] \quad 0 \le i \le 5, \tag{6.4}$$

where

$$\begin{aligned} \Xi \;=\; & 713097 q_2^3 + 44550 q_1^2 - 70\left(385 q_0 - 792 q_1 + 70\right) q_2 \\ & + 220990 q_2^2 - 7700 q_0 - 1400. \end{aligned} \tag{6.5}$$

Eqs. (6.3) and (6.4) naturally satisfy the conservation conditions defined by Eq. (3.42). Finally, in order to satisfy the stability condition defined by Eq. (3.17), the matrix $\tilde{\mathbf{M}} + \tilde{\mathbf{Q}}$, and all five of its upper-left square sub-matrices, must have positive determinants, leading to the following constraints on q_0, q_1, and q_3

$$\begin{aligned} & \frac{8}{15} q_2 + \frac{16}{105} > 0, \\ & -\frac{196}{75} q_2^3 + \frac{8}{135}\left(9 q_1 + 2\right) q_2 - \frac{56}{75} q_2^2 + \frac{16}{105} q_1 + \frac{32}{945} > 0, \\ & \frac{43218}{625} q_2^5 - \frac{28}{4125}\left(385 q_0 + 1287 q_1 + 532\right) q_2^3 + \frac{8036}{375} q_2^4 - \frac{216}{245} q_1^3 \\ & \quad + \frac{4}{7425}\left(8019 q_1^2 - 1386 q_0 - 8118 q_1 - 2056\right) q_2^2 + \frac{16}{1155}\left(11 q_0 + 2\right) q_1 - \frac{48}{245} q_1^2 \\ & \quad + \frac{8}{51975}\left(9\left(385 q_0 - 106\right) q_1 - 7128 q_1^2 + 770 q_0 + 140\right) q_2 + \frac{32}{945} q_0 + \frac{64}{10395} > 0. \end{aligned} \tag{6.6}$$

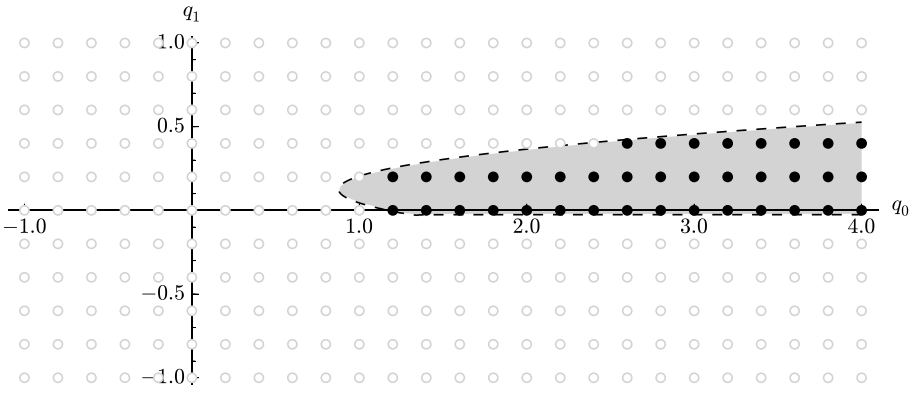

(a) $q_2 = -0.2$.

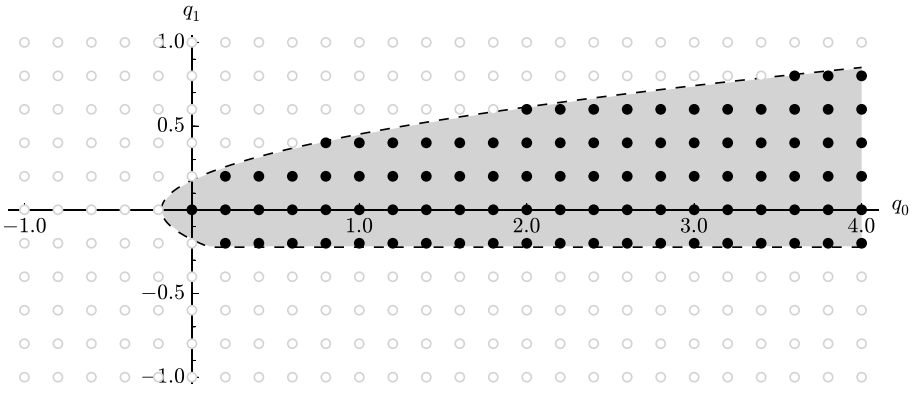

(b) $q_2 = 0.0$.

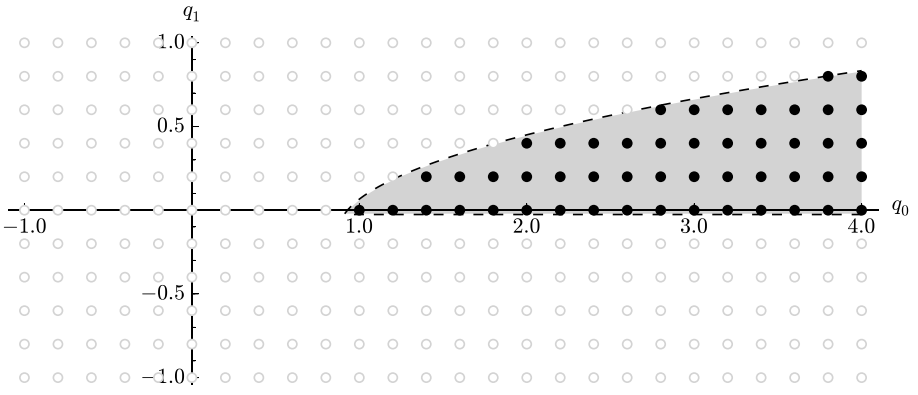

(c) $q_2 = 0.2$.

Fig. 3. Plots comparing theoretical and numerical results when $k = 5$. The shaded grey areas bounded by black dashed lines highlight the theoretically stable regions of $q_0 - q_1$ space with fixed $q_2 = -0.2$ (a), $q_2 = 0.0$ (b), and $q_2 = 0.2$ (c). Solid circles denote schemes that were found to be numerically stable. Hollow circles denote schemes that were found to be numerically unstable.

In summary, when $k = 5$, correction functions defined in terms of q_0, q_1, and q_2 via Eqs. (6.3) and (6.4) will result in stable FR schemes if q_0, q_1, and q_2 satisfy the constraints defined by Eq. (6.6). Examples of such correction functions are shown in Appendix A, Figs. 7–9. Also, for reference, the differential form of the norm defined by Eq. (3.32) when $k = 5$ is given in Appendix B, B.3.

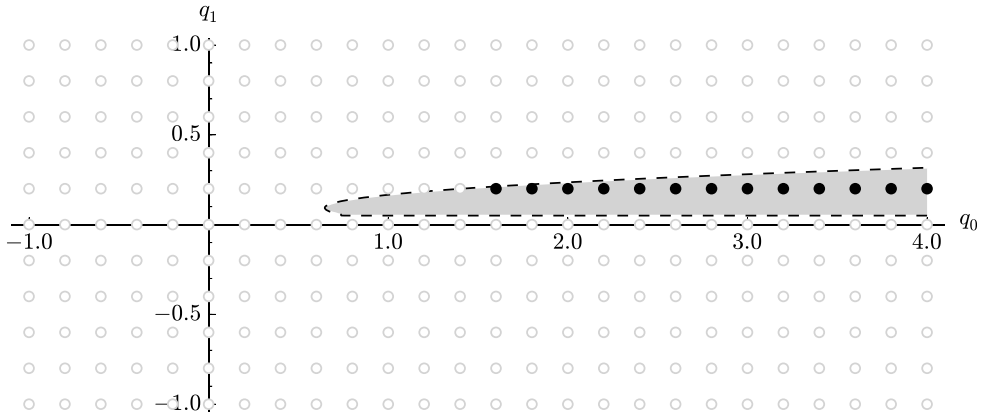

(a) $q_2 = -0.2$.

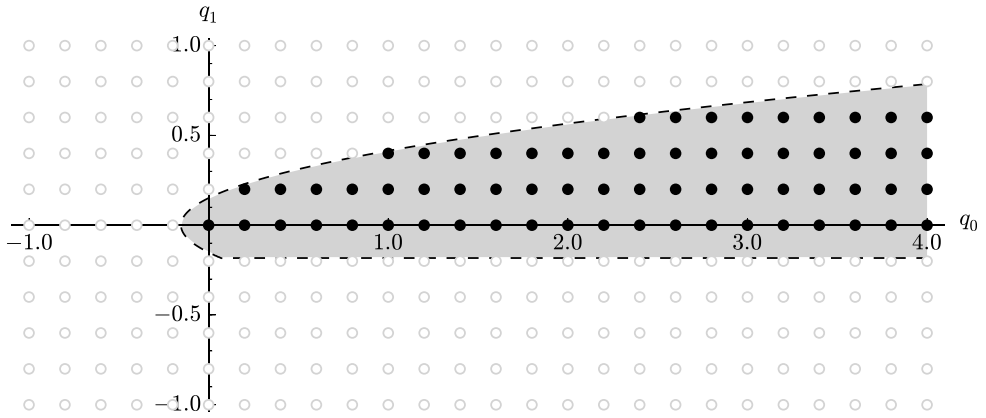

(b) $q_2 = 0.0$.

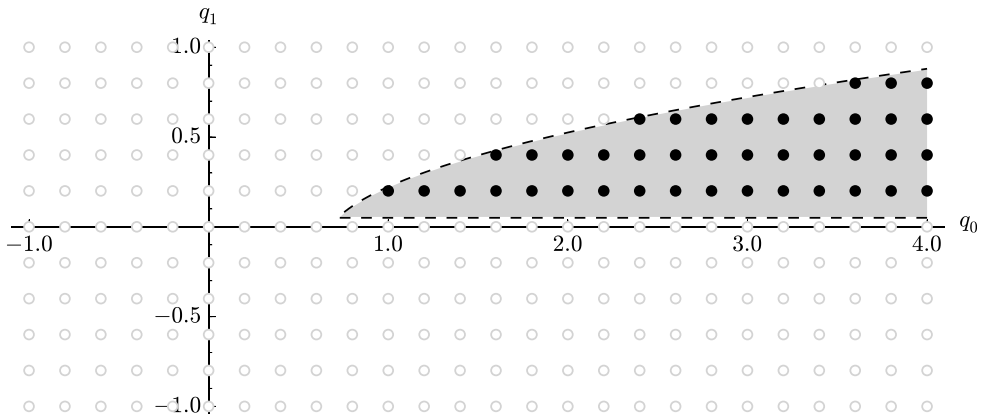

(c) $q_2 = 0.2$.

Fig. 4. Plots comparing theoretical and numerical results when $k = 6$. The shaded grey areas bounded by black dashed lines highlight the theoretically stable regions of $q_0 - q_1$ space with fixed $q_2 = -0.2$ (a), $q_2 = 0.0$ (b), and $q_2 = 0.2$ (c). Solid circles denote schemes that were found to be numerically stable. Hollow circles denote schemes that were found to be numerically unstable.

6.2. Recovery of Vincent–Castonguay–Jameson–Huynh schemes

If $q_1 = q_2 = 0$, then Eq. (6.3) collapses to

$$\begin{aligned} \mathbf{g}_{\hat{x}L}[0] &= -\frac{1}{2}, \qquad \mathbf{g}_{\hat{x}L}[1] = \frac{3}{2}, \qquad \mathbf{g}_{\hat{x}L}[2] = -\frac{5}{2}, \\ \mathbf{g}_{\hat{x}L}[3] &= \frac{7}{2}, \qquad \mathbf{g}_{\hat{x}L}[4] = -\frac{9}{2}, \qquad \mathbf{g}_{\hat{x}L}[5] = \frac{11}{11\,q_0 + 2}, \end{aligned} \tag{6.7}$$

and Eq. (6.6) collapses to

$$q_0 > -\frac{2}{11}. \tag{6.8}$$

These define VCJH correction functions for $k = 5$, parameterised by q_0, with $q_0 = 0$ recovering a DG scheme, $q_0 = 5/33$ recovering the energy-stable SD scheme described by Jameson [8], and $q_0 = 12/55$ recovering the g_2 described by Huynh [2]. We note that this description of a VCJH correction function, in terms of a modal Legendre expansion of its derivative, is similar to that presented previously by Huynh [10].

6.3. Numerical experiments

Numerical experiments were undertaken to demonstrate that, when $k = 5$, correction functions defined in terms of q_0, q_1 and q_2 via Eqs. (6.3) and (6.4) result in stable FR schemes if q_0, q_1 and q_2 satisfy the constraints defined by Eq. (6.6).

Specifically, an equispaced sampling of 1353 different schemes within a region of $q_0 - q_1 - q_2$ space bounded by $-1 \leq q_0 \leq 4$, $-1 \leq q_1 \leq 1$, and $-0.2 \leq q_2 \leq 0.2$ were used to solve Eq. (2.1) with the flux function defined by Eq. (4.9). For each of the 1353 numerical experiments the setup was identical to that described in Section 4.3. A scheme was deemed to be numerically unstable if the solution at any solution point attained a value of 1000 or greater before $t = 300$. Otherwise the scheme was deemed to be numerically stable. Plots illustrating which of the schemes were found to be numerically unstable, and which were found to be numerically stable, are shown in Fig. 3. Results of the numerical experiments are in agreement with the theoretical results of Section 6.1, since all schemes within the theoretically stable region of $q_0 - q_1 - q_2$ space, defined by Eq. (6.6), were found to be numerically stable. Additionally, it can be seen that all schemes outside of the theoretically stable region were found to be numerically unstable.

7. Identifying stable-symmetric-conservative correction functions when $k = 6$

7.1. Derivation

For reference, when $k = 6$

$$\tilde{\mathbf{M}} = \begin{bmatrix} 2 & 0 & 0 & 0 & 0 & 0 & 0 \\ 0 & \frac{2}{3} & 0 & 0 & 0 & 0 & 0 \\ 0 & 0 & \frac{2}{5} & 0 & 0 & 0 & 0 \\ 0 & 0 & 0 & \frac{2}{7} & 0 & 0 & 0 \\ 0 & 0 & 0 & 0 & \frac{2}{9} & 0 & 0 \\ 0 & 0 & 0 & 0 & 0 & \frac{2}{11} & 0 \\ 0 & 0 & 0 & 0 & 0 & 0 & \frac{2}{13} \end{bmatrix}, \qquad \tilde{\mathbf{D}} = \begin{bmatrix} 0 & 1 & 0 & 1 & 0 & 1 & 0 \\ 0 & 0 & 3 & 0 & 3 & 0 & 3 \\ 0 & 0 & 0 & 5 & 0 & 5 & 0 \\ 0 & 0 & 0 & 0 & 7 & 0 & 7 \\ 0 & 0 & 0 & 0 & 0 & 9 & 0 \\ 0 & 0 & 0 & 0 & 0 & 0 & 11 \\ 0 & 0 & 0 & 0 & 0 & 0 & 0 \end{bmatrix}. \tag{7.1}$$

By inspection, the most general form of $\tilde{\mathbf{Q}}$ that simultaneously satisfies the stability conditions defined by Eqs. (3.15) and (3.16), and the symmetry condition defined by Eq. (3.34), is

$$\tilde{\mathbf{Q}} = \begin{bmatrix} 0 & 0 & 0 & 0 & \\ 0 & 0 & 0 & 0 & \\ 0 & 0 & 0 & 0 & \\ 0 & 0 & 0 & q_3 & \cdots \\ 0 & 0 & -\frac{7}{5}q_3 & 0 & \\ 0 & \frac{21}{5}q_3 & 0 & -\frac{9}{7}q_2 - \frac{4}{5}q_3 & \\ -\frac{231}{5}q_3 & 0 & \frac{99}{35}q_2 + \frac{48}{5}q_3 & 0 & \end{bmatrix} \begin{bmatrix} 0 & 0 & -\frac{231}{5}q_3 \\ 0 & \frac{21}{5}q_3 & 0 \\ -\frac{7}{5}q_3 & 0 & \frac{99}{35}q_2 + \frac{48}{5}q_3 \\ 0 & -\frac{9}{7}q_2 - \frac{4}{5}q_3 & 0 \\ q_2 & 0 & -\frac{11}{9}q_1 - \frac{4}{7}q_2 - \frac{44}{45}q_3 \\ 0 & q_1 & 0 \\ \frac{11}{9}q_1 - \frac{4}{7}q_2 - \frac{44}{45}q_3 & 0 & q_0 \end{bmatrix}. \tag{7.2}$$

Substituting Eq. (7.2) into Eqs. (3.12) and (3.13) leads to

$$\begin{aligned} \mathbf{g}_{\hat{x}L}[0] &= \frac{189189\, q_3\, f(q_1,q_2,q_3)}{g(q_0,q_1,q_2,q_3)} - \frac{1}{2}, \\ \mathbf{g}_{\hat{x}R}[0] &= -\frac{189189\, q_3\, f(q_1,q_2,q_3)}{g(q_0,q_1,q_2,q_3)} + \frac{1}{2}, \end{aligned} \tag{7.3}$$

$$\mathbf{g}_{\hat{x}L}[1] = \mathbf{g}_{\hat{x}R}[1] = \frac{h(q_1,q_2,q_3)}{f(q_1,q_2,q_3)}, \tag{7.4}$$

where the specific forms of $f(q_1,q_2,q_3)$, $g(q_0,q_1,q_2,q_3)$ and $h(q_1,q_2,q_3)$ are omitted for brevity. In order for Eq. (7.3) to satisfy the conservation conditions defined by Eq. (3.42) it is required that $q_3 f(q_1,q_2,q_3) = 0$, which requires $q_3 = 0$ so that the denominator in (7.4) is non-zero. Substituting Eq. (7.2) into Eqs. (3.12) and (3.13) with $q_3 = 0$ leads to

$$\mathbf{g}_{\hat{x}L}[0] = -\frac{1}{2},$$

$$\mathbf{g}_{\hat{x}L}[1] = \frac{3}{2},$$

$$\mathbf{g}_{\hat{x}L}[2] = -\frac{35\left(55055\, q_1^2 - 9\,(4095\, q_0 - 19877\, q_1 - 1944)\, q_2 + 175851\, q_2^2 - 8190\, q_0 - 1260\right)}{\Xi},$$

$$\mathbf{g}_{\hat{x}L}[3] = -\frac{7\ (77\,q_1 + 99\,q_2 + 14)}{891\,q_2^2 - 154\,q_1 - 28},$$

$$\mathbf{g}_{\hat{x}L}[4] = -\frac{63\ \left(585\ (121\,q_1 - 8)\,q_2 + 196911\,q_2^2 - 8190\,q_0 - 10010\,q_1 - 1260\right)}{\Xi},$$

$$\mathbf{g}_{\hat{x}L}[5] = -\frac{77\ (9\,q_2 + 2)}{891\,q_2^2 - 154\,q_1 - 28},$$

$$\mathbf{g}_{\hat{x}L}[6] = -\frac{4095\ \left(891\,q_2^2 - 154\,q_1 - 28\right)}{\Xi},$$

(7.5)

and

$$\mathbf{g}_{\hat{x}R}[i] = (-1)^{i+1}\mathbf{g}_{\hat{x}L}[i] \quad 0 \le i \le 6,$$

(7.6)

where

$$\begin{aligned}\Xi \ =\ & 10320453\,q_2^3 + 770770\,q_1^2 - 630\ (819\,q_0 - 1144\,q_1 + 126)\,q_2 \\ & + 2461914\,q_2^2 - 114660\,q_0 - 17640.\end{aligned}$$

(7.7)

Finally, in order to satisfy the stability condition defined by Eq. (3.17), the matrix $\tilde{\mathbf{M}} + \tilde{\mathbf{Q}}$, and all six of its upper-left square sub-matrices, must have positive determinants, leading to the following constraints on q_0, q_1, and q_2

$$\begin{aligned}&\frac{16}{105}\,q_2 + \frac{32}{945} > 0,\\ &-\frac{216}{245}\,q_2^3 + \frac{16}{1155}\ (11\,q_1 + 2)\,q_2 - \frac{48}{245}\,q_2^2 + \frac{32}{945}\,q_1 + \frac{64}{10395} > 0,\\ &\frac{1058508}{60025}\,q_2^5 - \frac{24}{111475}\ (4095\,q_0 + 8437\,q_1 + 3204)\,q_2^3 + \frac{36072}{8575}\,q_2^4\\ &\quad - \frac{1936}{8505}\,q_1^3 + \frac{8}{525525}\left(86515\,q_1^2 - 12870\,q_0 - 47762\,q_1 - 10664\right)q_2^2\\ &\quad + \frac{16}{945945}\left(11\ (819\,q_0 - 82)\,q_1 - 12584\,q_1^2 + 1638\,q_0 + 252\right)q_2\\ &\quad + \frac{64}{10395}\,q_0 + \frac{32}{12285}\ (13\,q_0 + 2)\,q_1 - \frac{352}{8505}\,q_1^2 + \frac{128}{135135} > 0.\end{aligned}$$

(7.8)

In summary, when $k = 6$, correction functions defined in terms of q_0, q_1, and q_2 via Eqs. (7.5) and (7.6) will result in stable FR schemes if q_0, q_1, and q_2 satisfy the constraints defined by Eq. (7.8). Examples of such correction functions are shown in Appendix A, Figs. 10–12. Also, for reference, the differential form of the norm defined by Eq. (3.32) when $k = 6$ is given in Appendix B, B.4.

7.2. Recovery of Vincent–Castonguay–Jameson–Huynh Schemes

If $q_1 = q_2 = 0$, then Eq. (7.5) collapses to

$$\begin{aligned} \mathbf{g}_{\hat{x}L}[0] &= -\frac{1}{2}, \qquad \mathbf{g}_{\hat{x}L}[1] = \frac{3}{2}, \qquad \mathbf{g}_{\hat{x}L}[2] = -\frac{5}{2}, \\ \mathbf{g}_{\hat{x}L}[3] &= \frac{7}{2}, \qquad \mathbf{g}_{\hat{x}L}[4] = -\frac{9}{2}, \qquad \mathbf{g}_{\hat{x}L}[5] = \frac{11}{2}, \qquad \mathbf{g}_{\hat{x}L}[6] = -\frac{13}{13\,q_0 + 2}, \end{aligned} \tag{7.9}$$

and Eq. (7.8) collapses to

$$q_0 > -\frac{2}{13}. \tag{7.10}$$

These define VCJH correction functions for $k = 6$, parameterised by q_0, with $q_0 = 0$ recovering a DG scheme, $q_0 = 12/91$ recovering the energy-stable SD scheme described by Jameson [8], and $q_0 = 7/39$ recovering the g_2 described by Huynh [2]. We note that this description of a VCJH correction function, in terms of a modal Legendre expansion of its derivative, is similar to that presented previously by Huynh [10].

7.3. Numerical experiments

Numerical experiments were undertaken to demonstrate that, when $k = 6$, correction functions defined in terms of q_0, q_1 and q_2 via Eqs. (7.5) and (7.6) result in stable FR schemes if q_0, q_1 and q_2 satisfy the constraints defined by Eq. (7.8).

Specifically, an equispaced sampling of 1353 different schemes within a region of $q_0 - q_1 - q_2$ space bounded by $-1 \leq q_0 \leq 4$, $-1 \leq q_1 \leq 1$, and $-0.2 \leq q_2 \leq 0.2$ were used to solve Eq. (2.1) with the flux function defined by Eq. (4.9). For each of the 1353 numerical experiments the setup was identical to that described in Section 4.3. A scheme was deemed to be numerically unstable if the solution at any solution point attained a value of 1000 or greater before $t = 300$. Otherwise the scheme was deemed to be numerically stable. Plots illustrating which of the schemes were found to be numerically unstable, and which were found to be numerically stable, are shown in Fig. 4. Results of the numerical experiments are in agreement with the theoretical results of Section 7.1, since all schemes within the theoretically stable region of $q_0 - q_1 - q_2$ space, defined by Eq. (7.8), were found to be numerically stable. Additionally, it can be seen that all schemes outside of the theoretically stable region were found to be numerically unstable.

8. Conclusions

Building on the work of Huynh [2] and Jameson [8], Vincent, Castonguay and Jameson recently identified a one-parameter family of VCJH correction functions that lead to stable FR schemes for 1D linear advection problems [7]. In this study we developed a procedure for identifying an extended range of stable, symmetric, and conservative FR correction functions. The procedure was applied to identify ranges of such correction functions for various orders of accuracy. In all cases the original one-parameter VCJH correction functions were found to be a subset of the extended ranges. Numerical experiments were undertaken, and the results found to be in agreement with the theoretical findings. Future studies should extend the approach presented here to simplex elements in 2D and 3D.

Acknowledgements

The authors would like to thank the Engineering and Physical Sciences Research Council for their support via grants EP/K027379/1, EP/L000407/1, EP/M50676X/1 and two Doctoral Training Grants. The authors would also like to thank the Air Force Office of Scientific Research for support via grant FA9550-10-1-0418, and the National Science Foundation for support via grant 1114816. Finally, the authors would like to thank Dr. Andrew Wynn for useful discussions.

Appendix A. Correction functions

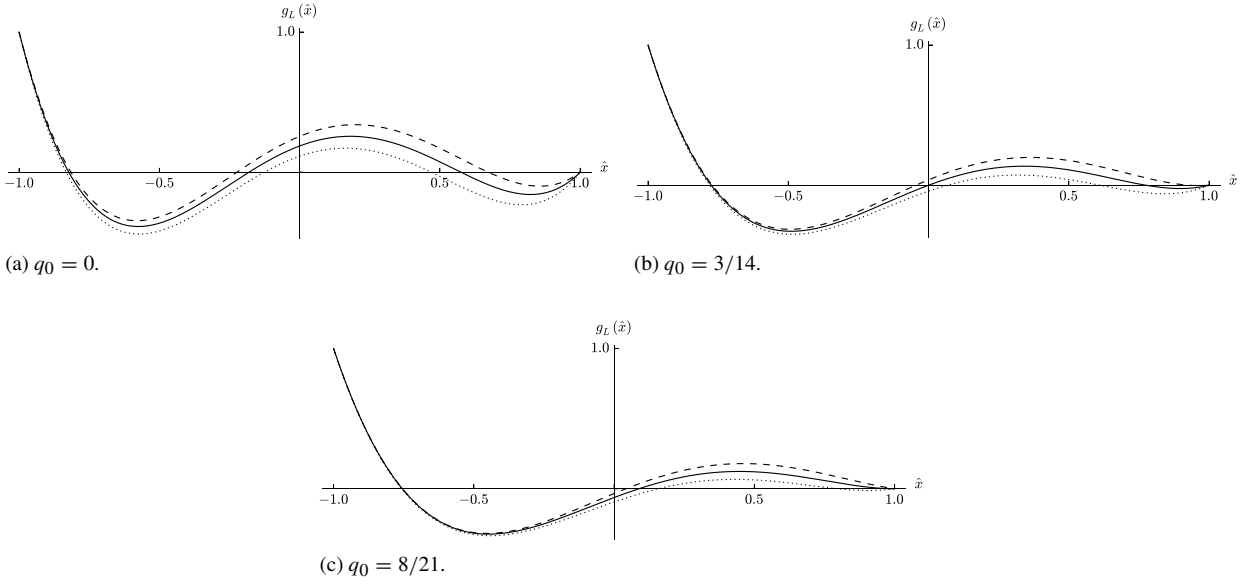

(a) $q_0 = 0$.

(b) $q_0 = 3/14$.

(c) $q_0 = 8/21$.

Fig. 5. Plots of left correction functions g_L when $k = 3$ with $q_0 = 0$ (a), $q_0 = 3/14$ (b), $q_0 = 8/21$ (c). For each plot $q_1 = -3/140$ (dashed lines), $q_1 = 0$ (solid lines), $q_1 = 3/140$ (dotted lines).

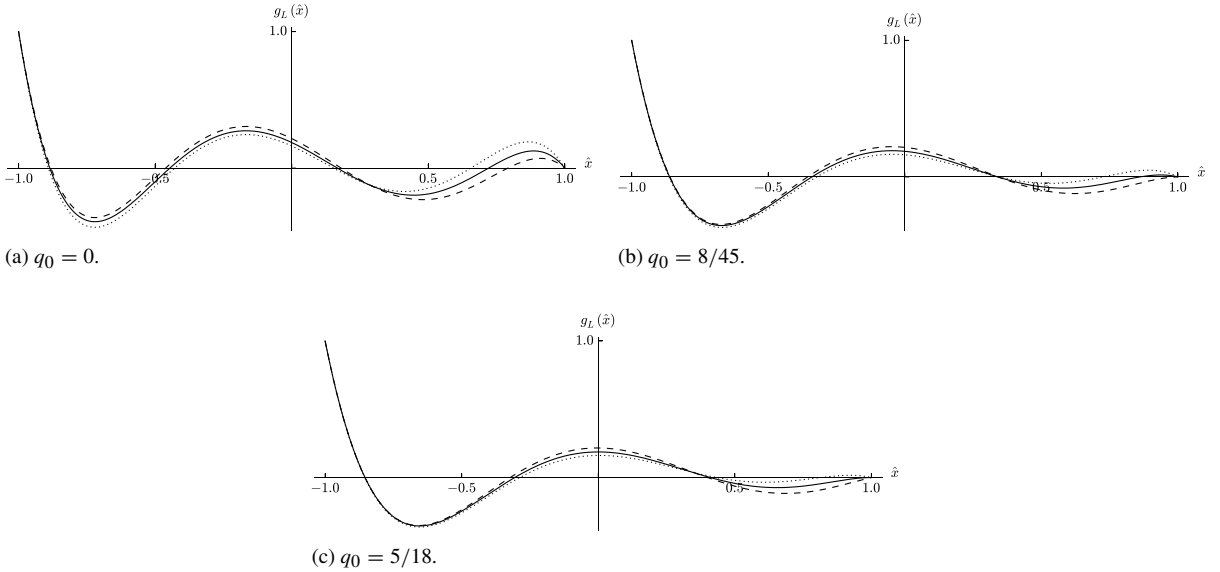

(a) $q_0 = 0$.

(b) $q_0 = 8/45$.

(c) $q_0 = 5/18$.

Fig. 6. Plots of left correction functions g_L when $k = 4$ with $q_0 = 0$ (a), $q_0 = 8/45$ (b), $q_0 = 5/18$ (c). For each plot $q_1 = -8/450$ (dashed lines), $q_1 = 0$ (solid lines), $q_1 = 8/450$ (dotted lines).

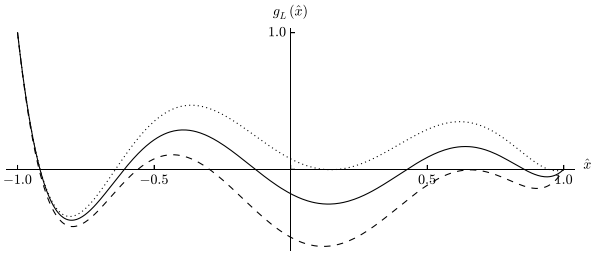

(a) $q_0 = 0$.

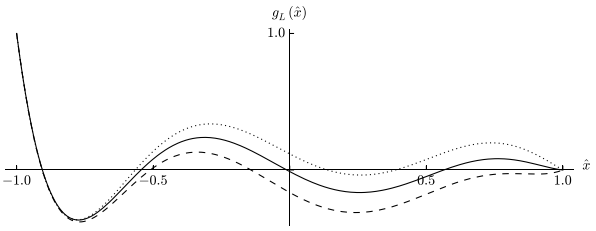

(b) $q_0 = 5/33$.

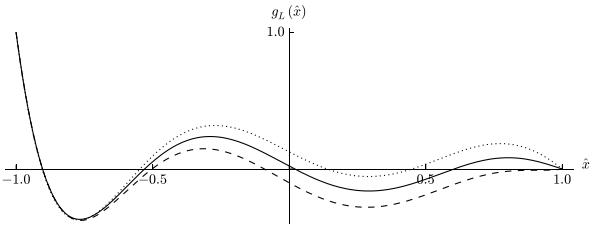

(c) $q_0 = 12/55$.

Fig. 7. Plots of left correction functions g_L when $k = 5$ with $q_0 = 0$ (a), $q_0 = 5/33$ (b), $q_0 = 12/55$ (c). For each plot $q_1 = -5/330$, and $q_2 = -5/330$ (dashed lines), $q_2 = 0$ (solid lines), $q_2 = 5/330$ (dotted lines).

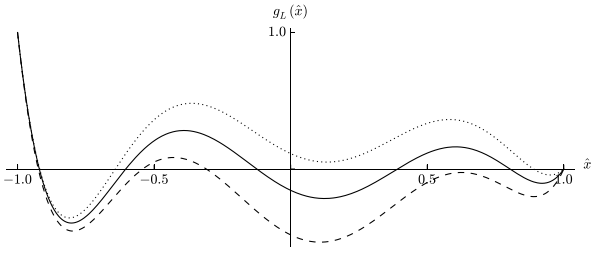

(a) $q_0 = 0$.

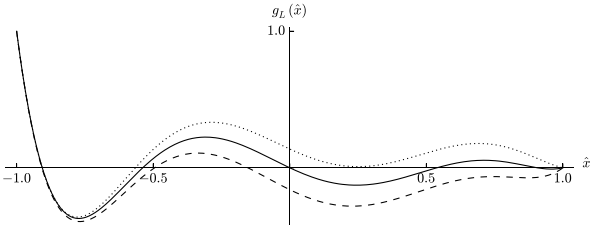

(b) $q_0 = 5/33$.

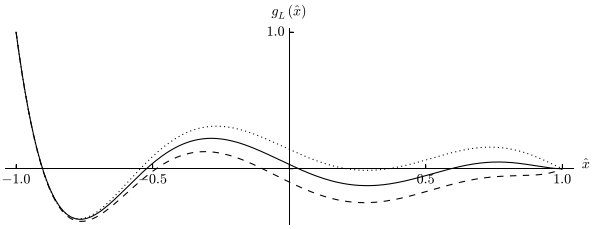

(c) $q_0 = 12/55$.

Fig. 8. Plots of left correction functions g_L when $k = 5$ with $q_0 = 0$ (a), $q_0 = 5/33$ (b), $q_0 = 12/55$ (c). For each plot $q_1 = 0$, and $q_2 = -5/330$ (dashed lines), $q_2 = 0$ (solid lines), $q_2 = 5/330$ (dotted lines).

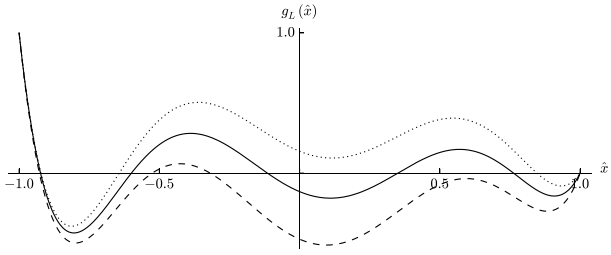

(a) $q_0 = 0$.

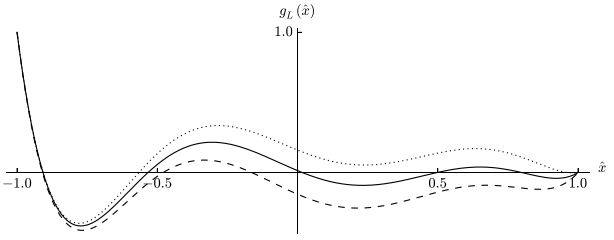

(b) $q_0 = 5/33$.

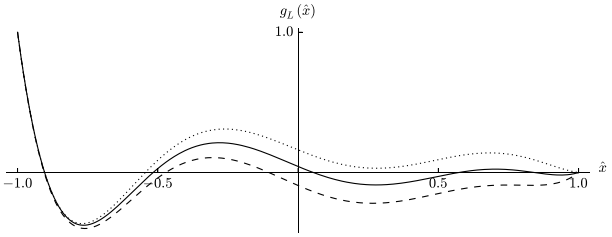

(c) $q_0 = 12/55$.

Fig. 9. Plots of left correction functions g_L when $k = 5$ with $q_0 = 0$ (a), $q_0 = 5/33$ (b), $q_0 = 12/55$ (c). For each plot $q_1 = 5/330$, and $q_2 = -5/330$ (dashed lines), $q_2 = 0$ (solid lines), $q_2 = 5/330$ (dotted lines).

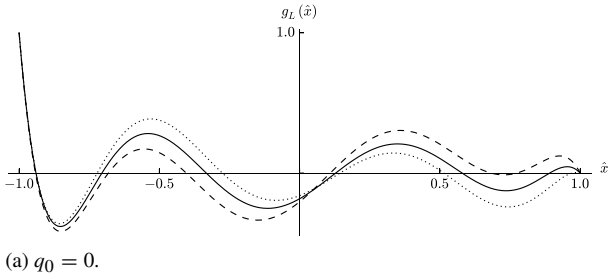

(a) $q_0 = 0$.

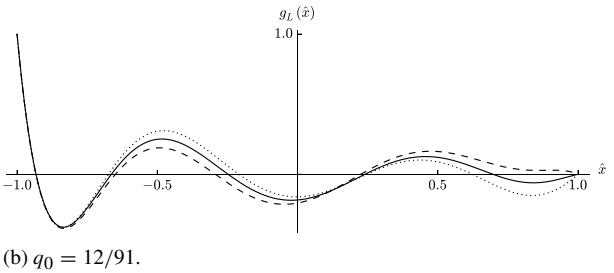

(b) $q_0 = 12/91$.

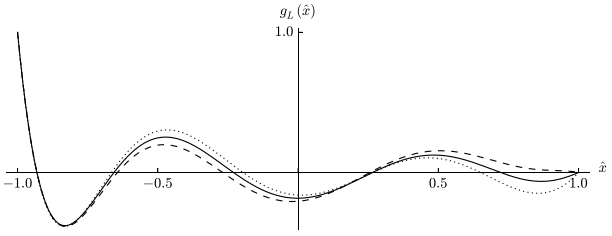

(c) $q_0 = 7/39$.

Fig. 10. Plots of left correction functions g_L when $k = 6$ with $q_0 = 0$ (a), $q_0 = 12/91$ (b), $q_0 = 7/39$ (c). For each plot $q_1 = -12/910$, and $q_2 = -12/910$ (dashed lines), $q_2 = 0$ (solid lines), $q_2 = 12/910$ (dotted lines).

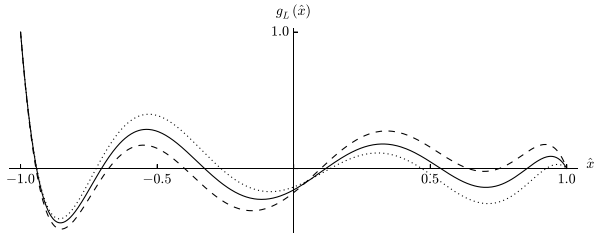

(a) $q_0 = 0$.

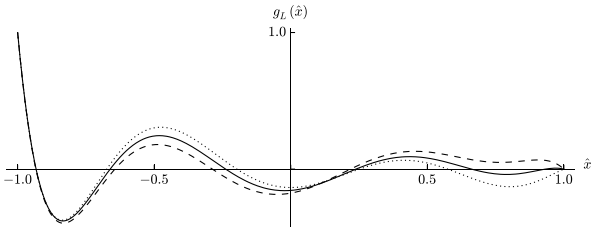

(b) $q_0 = 12/91$.

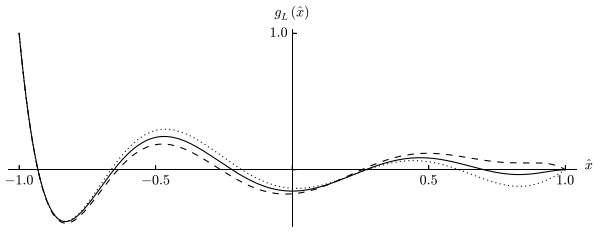

(c) $q_0 = 7/39$.

Fig. 11. Plots of left correction functions g_L when $k = 6$ with $q_0 = 0$ (a), $q_0 = 12/91$ (b), $q_0 = 7/39$ (c). For each plot $q_1 = 0$, and $q_2 = -12/910$ (dashed lines), $q_2 = 0$ (solid lines), $q_2 = 12/910$ (dotted lines).

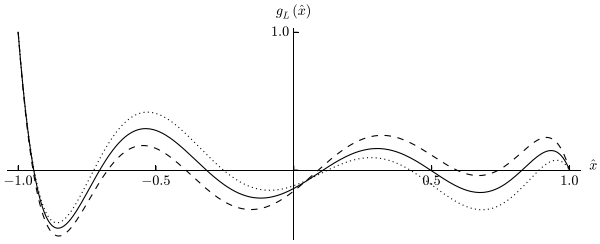

(a) $q_0 = 0$.

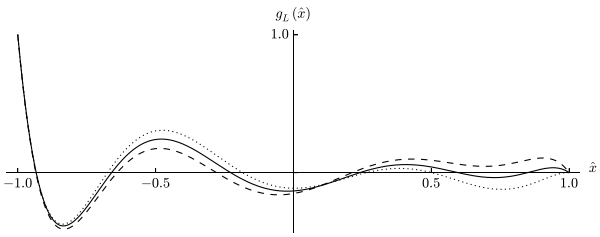

(b) $q_0 = 12/91$.

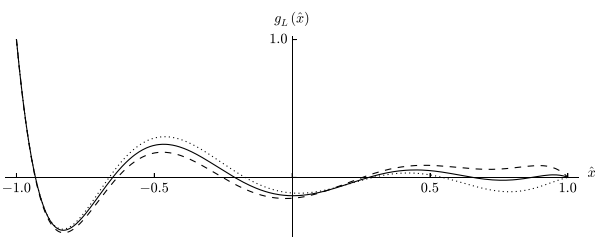

(c) $q_0 = 7/39$.

Fig. 12. Plots of left correction functions g_L when $k = 6$ with $q_0 = 0$ (a), $q_0 = 12/91$ (b), $q_0 = 7/39$ (c). For each plot $q_1 = 12/910$, and $q_2 = -12/910$ (dashed lines), $q_2 = 0$ (solid lines), $q_2 = 12/910$ (dotted lines).

Appendix B. Differential form of norms

B.1. $k = 3$

When $k = 3$, $\tilde{\mathbf{M}} + \tilde{\mathbf{Q}}$ can be decomposed as

$$\tilde{\mathbf{M}} + \tilde{\mathbf{Q}} = \tilde{\mathbf{M}} - \epsilon_1(\tilde{\mathbf{D}}^T\tilde{\mathbf{M}}\tilde{\mathbf{D}}^3 + \tilde{\mathbf{D}}^{T3}\tilde{\mathbf{M}}\tilde{\mathbf{D}}) + \epsilon_2\tilde{\mathbf{D}}^{T2}\tilde{\mathbf{M}}\tilde{\mathbf{D}}^2 + \epsilon_3\tilde{\mathbf{D}}^{T3}\tilde{\mathbf{M}}\tilde{\mathbf{D}}^3, \tag{B.1}$$

where

$$\begin{aligned}\epsilon_1 &= \epsilon_2 = \frac{q_1}{18},\\ \epsilon_3 &= \frac{q_0 - 5q_1}{450}.\end{aligned} \tag{B.2}$$

Hence, $\|u^\delta\|$ can be written in differential form as

$$\|u^\delta\| = \sqrt{\sum_{n=0}^{N-1}\int_{x_n}^{x_{n+1}} (u_n^\delta)^2 - \frac{2\epsilon_1}{J_n^4}\frac{\mathrm{d}u_n^\delta}{\mathrm{d}x}\frac{\mathrm{d}^3u_n^\delta}{\mathrm{d}x^3} + \frac{\epsilon_2}{J_n^4}\left(\frac{\mathrm{d}^2u_n^\delta}{\mathrm{d}x^2}\right)^2 + \frac{\epsilon_3}{J_n^6}\left(\frac{\mathrm{d}^3u_n^\delta}{\mathrm{d}x^3}\right)^2 \mathrm{d}x}. \tag{B.3}$$

B.2. $k = 4$

When $k = 4$, $\tilde{\mathbf{M}} + \tilde{\mathbf{Q}}$ can be decomposed as

$$\tilde{\mathbf{M}} + \tilde{\mathbf{Q}} = \tilde{\mathbf{M}} - \epsilon_1(\tilde{\mathbf{D}}^{T2}\tilde{\mathbf{M}}\tilde{\mathbf{D}}^4 + \tilde{\mathbf{D}}^{T4}\tilde{\mathbf{M}}\tilde{\mathbf{D}}^2) + \epsilon_2\tilde{\mathbf{D}}^{T3}\tilde{\mathbf{M}}\tilde{\mathbf{D}}^3 + \epsilon_3\tilde{\mathbf{D}}^{T4}\tilde{\mathbf{M}}\tilde{\mathbf{D}}^4, \tag{B.4}$$

where

$$\begin{aligned}\epsilon_1 &= \epsilon_2 = \frac{q_1}{450},\\ \epsilon_3 &= \frac{q_0 - 7q_1}{22050}.\end{aligned} \tag{B.5}$$

Hence, $\|u^\delta\|$ can be written in differential form as

$$\|u^\delta\| = \sqrt{\sum_{n=0}^{N-1}\int_{x_n}^{x_{n+1}} (u_n^\delta)^2 - \frac{2\epsilon_1}{J_n^6}\frac{\mathrm{d}^2u_n^\delta}{\mathrm{d}x^2}\frac{\mathrm{d}^4u_n^\delta}{\mathrm{d}x^4} + \frac{\epsilon_2}{J_n^6}\left(\frac{\mathrm{d}^3u_n^\delta}{\mathrm{d}x^3}\right)^2 + \frac{\epsilon_3}{J_n^8}\left(\frac{\mathrm{d}^4u_n^\delta}{\mathrm{d}x^4}\right)^2 \mathrm{d}x}. \tag{B.6}$$

B.3. $k = 5$

When $k = 5$, $\tilde{\mathbf{M}} + \tilde{\mathbf{Q}}$ can be decomposed as

$$\begin{aligned}\tilde{\mathbf{M}} + \tilde{\mathbf{Q}} = \tilde{\mathbf{M}} &+ \epsilon_1(\tilde{\mathbf{D}}^T\tilde{\mathbf{M}}\tilde{\mathbf{D}}^5 + \tilde{\mathbf{D}}^{T5}\tilde{\mathbf{M}}\tilde{\mathbf{D}}) - \epsilon_2(\tilde{\mathbf{D}}^{T2}\tilde{\mathbf{M}}\tilde{\mathbf{D}}^4 + \tilde{\mathbf{D}}^{T4}\tilde{\mathbf{M}}\tilde{\mathbf{D}}^2)\\ &+ \epsilon_3\tilde{\mathbf{D}}^{T3}\tilde{\mathbf{M}}\tilde{\mathbf{D}}^3 - \epsilon_4(\tilde{\mathbf{D}}^{T3}\tilde{\mathbf{M}}\tilde{\mathbf{D}}^5 + \tilde{\mathbf{D}}^{T5}\tilde{\mathbf{M}}\tilde{\mathbf{D}}^3) + \epsilon_5\tilde{\mathbf{D}}^{T4}\tilde{\mathbf{M}}\tilde{\mathbf{D}}^4 + \epsilon_6\tilde{\mathbf{D}}^{T5}\tilde{\mathbf{M}}\tilde{\mathbf{D}}^5,\end{aligned} \tag{B.7}$$

where

$$\begin{aligned}\epsilon_1 &= \epsilon_2 = \epsilon_3 = \frac{q_2}{450},\\ \epsilon_4 &= \epsilon_5 = \frac{q_1 - 7q_2}{22050},\\ \epsilon_6 &= \frac{q_0 - 9q_1 + 35q_2}{1786050}.\end{aligned} \tag{B.8}$$

Hence, $\|u^\delta\|$ can be written in differential form as

$$\begin{aligned}\|u^\delta\| = \sqrt{\sum_{n=0}^{N-1}\int_{x_n}^{x_{n+1}} (u_n^\delta)^2 + \frac{2\epsilon_1}{J_n^6}\frac{\mathrm{d}u_n^\delta}{\mathrm{d}x}\frac{\mathrm{d}^5u_n^\delta}{\mathrm{d}x^5} - \frac{2\epsilon_2}{J_n^6}\frac{\mathrm{d}^2u_n^\delta}{\mathrm{d}x^2}\frac{\mathrm{d}^4u_n^\delta}{\mathrm{d}x^4} + \frac{\epsilon_3}{J_n^6}\left(\frac{\mathrm{d}^3u_n^\delta}{\mathrm{d}x^3}\right)^2}\\ \sqrt{- \frac{2\epsilon_4}{J_n^8}\frac{\mathrm{d}^3u_n^\delta}{\mathrm{d}x^3}\frac{\mathrm{d}^5u_n^\delta}{\mathrm{d}x^5} + \frac{\epsilon_5}{J_n^8}\left(\frac{\mathrm{d}^4u_n^\delta}{\mathrm{d}x^4}\right)^2 + \frac{\epsilon_6}{J_n^{10}}\left(\frac{\mathrm{d}^5u_n^\delta}{\mathrm{d}x^5}\right)^2 \mathrm{d}x}.\end{aligned} \tag{B.9}$$

B.4. $k = 6$

When $k = 6$, $\tilde{\mathbf{M}} + \tilde{\mathbf{Q}}$ can be decomposed as

$$\begin{aligned}\tilde{\mathbf{M}} + \tilde{\mathbf{Q}} = \tilde{\mathbf{M}} &+ \epsilon_1(\tilde{\mathbf{D}}^{T2}\tilde{\mathbf{M}}\tilde{\mathbf{D}}^6 + \tilde{\mathbf{D}}^{T6}\tilde{\mathbf{M}}\tilde{\mathbf{D}}^2) - \epsilon_2(\tilde{\mathbf{D}}^{T3}\tilde{\mathbf{M}}\tilde{\mathbf{D}}^5 + \tilde{\mathbf{D}}^{T5}\tilde{\mathbf{M}}\tilde{\mathbf{D}}^3) \\ &+ \epsilon_3\tilde{\mathbf{D}}^{T4}\tilde{\mathbf{M}}\tilde{\mathbf{D}}^4 - \epsilon_4(\tilde{\mathbf{D}}^{T4}\tilde{\mathbf{M}}\tilde{\mathbf{D}}^5 + \tilde{\mathbf{D}}^{T5}\tilde{\mathbf{M}}\tilde{\mathbf{D}}^4) + \epsilon_5\tilde{\mathbf{D}}^{T5}\tilde{\mathbf{M}}\tilde{\mathbf{D}}^5 + \epsilon_6\tilde{\mathbf{D}}^{T6}\tilde{\mathbf{M}}\tilde{\mathbf{D}}^6,\end{aligned} \tag{B.10}$$

where

$$\begin{aligned}\epsilon_1 &= \epsilon_2 = \epsilon_3 = \frac{q_2}{22050}, \\ \epsilon_4 &= \epsilon_5 = \frac{q_1 - 9q_2}{1786050}, \\ \epsilon_6 &= \frac{q_0 - 11q_1 + 54q_2}{216112050}.\end{aligned} \tag{B.11}$$

Hence, $\|u^\delta\|$ can be written in differential form as

$$\|u^\delta\| = \sqrt{\sum_{n=0}^{N-1}\int_{x_n}^{x_{n+1}} (u_n^\delta)^2 + \frac{2\epsilon_1}{J_n^8}\frac{\mathrm{d}^2u_n^\delta}{\mathrm{d}x^2}\frac{\mathrm{d}^6u_n^\delta}{\mathrm{d}x^6} - \frac{2\epsilon_2}{J_n^8}\frac{\mathrm{d}^3u_n^\delta}{\mathrm{d}x^3}\frac{\mathrm{d}^5u_n^\delta}{\mathrm{d}x^5} + \frac{\epsilon_3}{J_n^8}\left(\frac{\mathrm{d}^4u_n^\delta}{\mathrm{d}x^4}\right)^2 - \frac{2\epsilon_4}{J_n^{10}}\frac{\mathrm{d}^4u_n^\delta}{\mathrm{d}x^4}\frac{\mathrm{d}^6u_n^\delta}{\mathrm{d}x^6} + \frac{\epsilon_5}{J_n^{10}}\left(\frac{\mathrm{d}^5u_n^\delta}{\mathrm{d}x^5}\right)^2 + \frac{\epsilon_6}{J_n^{12}}\left(\frac{\mathrm{d}^6u_n^\delta}{\mathrm{d}x^6}\right)^2 \mathrm{d}x}. \tag{B.12}$$

References

[1] P.E. Vincent, A. Jameson, Facilitating the adoption of unstructured high-order methods amongst a wider community of fluid dynamicists, Math. Model. Nat. Phenom. 6 (2011) 97.
[2] H.T. Huynh, A flux reconstruction approach to high-order schemes including discontinuous Galerkin methods, AIAA Paper 2007-4079 (2007).
[3] Z.J. Wang, H. Gao, A unifying lifting collocation penalty formulation including the discontinuous Galerkin, spectral volume/difference methods for conservation laws on mixed grids, J. Comput. Phys. 228 (2009) 8161.
[4] H.T. Huynh, Z.J. Wang, P.E. Vincent, High-order methods for computational fluid dynamics: a brief review of compact differential formulations on unstructured grids, Comput. Fluids 98 (2014) 209.
[5] P.E. Vincent, P. Castonguay, A. Jameson, Insights from von Neumann analysis of high-order flux reconstruction schemes, J. Comput. Phys. 230 (2011) 8134.
[6] K. Asthana, A. Jameson, High-order flux reconstruction schemes with minimal dispersion and dissipation, J. Sci. Comput. (2014).
[7] P.E. Vincent, P. Castonguay, A. Jameson, A new class of high-order energy stable flux reconstruction schemes, J. Sci. Comput. 47 (2011) 50.
[8] A. Jameson, A proof of the stability of the spectral difference method for all orders of accuracy, J. Sci. Comput. 45 (2010) 348.
[9] P.L. Roe, Approximate Riemann solvers, parameter vectors, and difference schemes, J. Comput. Phys. 43 (1981) 357.
[10] H.T. Huynh, On Formulations of Discontinuous Galerkin and Related Methods for Conservation Laws, Technical Report TM 218135, NASA, NASA Glenn Research Center, 2014.
[11] M.H. Carpenter, C. Kennedy, Fourth-order 2N-storage Runge–Kutta Schemes, Tech. Rep. TM 109112, NASA, NASA Langley Research Center, 1994.